Fall 2023

A New View of Chlorophyll Dynamics in the Southern Mid-Atlantic Bight from a Two-Year High-Resolution Spray Glider Survey

Francesco Lane
Old Dominion University

A NEW VIEW OF CHLOROPHYLL DYNAMICS IN THE SOUTHERN MID-ATLANTIC BIGHT FROM A TWO YEAR HIGH-RESOLUTION SPRAY GLIDER SURVEY

by

Francesco Lane
B.S. August 2018, University of Florida

A Thesis Submitted to the Faculty of
Old Dominion University in Partial Fulfillment of the
Requirement for the Degree of

MASTER OF SCIENCE

OCEAN AND EARTH SCIENCES

OLD DOMINION UNIVERSITY
December 2023

Approved by:

Margaret R. Mulholland (Director)

Sophie Clayton (Member)

Eileen E. Hofmann (Member)

ABSTRACT

A NEW VIEW OF CHLOROPHYLL DYNAMICS IN THE SOUTHERN MID-ATLANTIC BIGHT FROM A TWO YEAR HIGH-RESOLUTION SPRAY GLIDER SURVEY

Francesco Lane
Old Dominion University, 2023
Director: Dr. Margaret R. Mulholland

The southern Mid-Atlantic Bight (MAB) near Cape Hatteras, NC, USA, is likely a hotspot for the episodic export of carbon-rich shelf waters to the open ocean. Over a 2 year period, from March 2017 to May 2019, Spray gliders repeatedly occupied transects, along the slope and across the shelf, generating high-resolution chlorophyll fluorescence (fChl) data in the southern MAB. This study implements an fChl calibration method utilizing remotely sensing ocean color as a standard. We validate the method's utility by demonstrating a reduction in post-calibration cross-mission fChl variability and demonstrating close correspondence between the calibrated fChl data and an *in situ* chlorophyll measurements. Using the calibrated fChl data, we calculate the mean and standard deviation of fChl for the study region on both annual and seasonal time scales. In general, we found that fChl concentrations were highest in the winter-spring season, followed by the summer, with the lowest mean fChl observed in fall. Spatially, high mean concentrations of fChl are associated with a relatively greater chlorophyll at depth in spring-winter, from the surface down to 250 m. High mean concentrations of fChl are confined to a subsurface layer from 10 m to 40 m in the summer, and fall's highest mean concentrations of fChl are found in the top 50 m in fall. The highest variability in fChl was observed in the winter-spring season, with peaks near the surface and between 150m and 250m at the southern end of

the slope transect, near the Gulf Stream wall. We interpret this high variability in fChl as an indication that episodic fluxes of high chlorophyll concentrations, termed as “deep chlorophyll events”, may be occurring in this location. To support this idea, we identified 10 individual deep chlorophyll events based on fChl (> 0.75 mg m^{-3}) and depth (>100m) thresholds and found that the events occurred primarily in winter-spring; with a small number also identified in summer and none in fall; and have similarities with previously recognized mechanisms of shelf water cascade dynamics and MAB cold pool export.

This thesis is dedicated to those of you who see the world and intend to be in harmony with it.

ACKNOWLEDGMENTS

I would like to acknowledge the people who helped make this possible. I would not have been able to accomplish this project without their mentorship. My mentors have supported me to approach this complex workflow in a stepwise manner and become an effective, granular part of the immense initiative to understand ocean systems.

To Dr. Sophie Clayton, my advisor, for pulling as much clarity and improvement out of my scientific communication as I think is humanly possible. She put in long hours of meetings and reviewing to support me in accomplishing this abstract endeavor of actualizing science and humanitarian knowledge.

To Dr. Robert E. Todd, for providing me the opportunity to work with the PEACH Spray glider data. He and Dr. Clayton helped me constrain and develop the scope of my interpretation with the evidence I had generated, a lesson in applied data sciences in complex natural systems which cannot be understated.

To Old Dominion University's Ocean and Earth Science Department, the opportunity you gave me to write this thesis is foundational in my ability to contribute to humanitarian goals through science. In this day or any day, there is really no greater gift.

Sincere gratitude,

Francesco Lane

TABLE OF CONTENTS

Page

LIST OF TABLES

Table Page

LIST OF FIGURES

Figure Page

CHAPTER 1

INTRODUCTION

Quantifying carbon exchange between carbon rich coastal systems and the oligotrophic open ocean, as well as its alteration due to changing climate, is essential to accurately predict how ocean and global carbon budgets will be impacted by anthropogenic climate change (Bauer et al., 2013). Compared to the open ocean, continental shelves are characterized by higher particulate organic carbon concentrations and elevated rates of primary production. Results of the shelf edge exchange process program rejected the hypothesis that most of this carbon is exported from the shelf, finding evidence it is recycled in net community production on the shelf (Biscaye et al., 1994). Of the total carbon flux leaving the neritic zone of Eastern North America, which remains unconstrained in our global carbon budget predictions, a Mid-Atlantic Bight (MAB) carbon budget model estimated that 80% ± 9% is exported to the open ocean using a residual of the other domain fluxes, including burial and atmosphere-sea exchange (Najjar et al., 2018). Furthermore, a biogeochemical numerical MAB nitrogen budget model found that strong interannual variability in net community production that drives the recycling of carbon on shelf was primarily influenced by along and across shelf horizontal nutrient fluxes; with strongest magnitudes of annual net community production occurring in the southern MAB appearing to be linked with spatiotemporal variability of the Gulf Stream (GS) and the slope water gyre (Fredrichs et al., 2018). Considering the results from the previous investigations, more comprehensive observational studies are essential to constrain shelf-open ocean biogeochemical exchange linked to climate feedback.

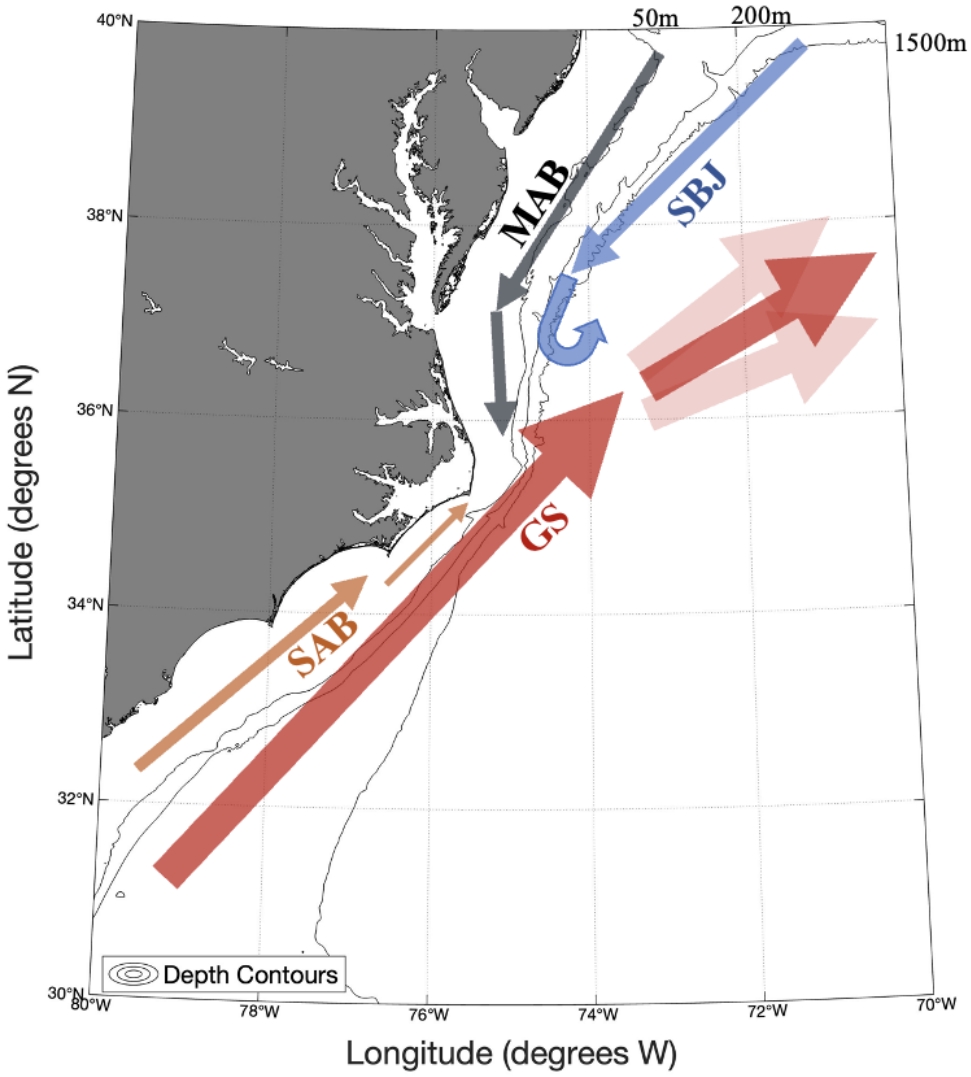

Figure 1. Map of Converging Water Masses in the southern Mid-Atlantic Bight (MAB) off the U.S. mid-Atlantic coast with 50, 200, and 1500 m isobaths as thin black contours off the coast, from left to right respectively. Schematic surface currents shown as arrows entering the region are the Gulf Stream (GS) shown in dark red, the shelfbreak jet (SBJ) shown in blue, the flow over the MAB in black, and the South Atlantic Bight (SAB) shown in orange.

Hydrographic water mass dynamics in the southern MAB, off Cape Hatteras, NC, USA, are complex and characterized by the convergence of highly productive coastal shelf waters from the MAB and South Atlantic Bight, the shelfbreak jet, and oligotrophic western boundary current GS waters (Figure 1). The fine scale processes driving cross-shelf exchange of carbon-rich waters are still poorly understood. The southern MAB domain is confined by two ocean circulation barriers: the shelfbreak front to the east and the GS wall to the south where the MAB converges with the South Atlantic Bight. Mean estimates of water mass distributions put the mean frontal wall of the GS occurring at the southern end of the PEACH study area, located at ~35.75°N. This front is visible in those annual mean hydrographic fields as a horizontal gradient in salinity extending from the surface to 100 meters depth. About 20-25 km north of the front, the gliders observed the surface point of mean alongshore convergence. This convergence point adjacent to the GS wall was concomitant with net export of shelf waters to the open ocean. This export is dominated by episodic events, where 50% of export occurred in major events with volumes greater than 1 standard deviation above the mean within 17% of the time (Todd, 2020a). Within that episodic export event hotspot, Han et al. (2021) observed one event when winter atmospheric cooling over the shelf, adjacent to a relatively low-density GS filament on the slope, led to the subduction via a density-driven gravity current of shelf water. This shelf water contained high chlorophyll and dissolved oxygen concentrations and was subsequently entrained northeastward below the GS (Han et al., 2021). This cascading of dense shelf waters downslope represents an irreversible removal process, that occurs globally, exporting particulate organic carbon produced on the highly productive shelves to the deep oligotrophic open ocean, where it can be sequestered, that are difficult to observe due to their intermittent character (Shapiro et al., 2003 and Ivanov et al., 2004). It is still unknown how frequent these cascading carbon-rich

export events are in the southern MAB due to a lack of continuous, highly spatially and temporally resolved biogeochemical data, but they likely play an important role in exporting large quantities of coastal carbon to the deep open ocean (Huthnance, 1995). The impact of regional episodic export on biogeochemical mechanisms, like shelf water cascades, in this region and the greater North American coastal boundary, in particular the transport of chlorophyll and carbon from the shelf to the open ocean, are still not well understood and remain largely unconstrained.

Biogeochemical surveys are required to observe the distribution of continental shelf phytoplankton, the community's primary producers, in relation to physical hydrographic shelf-open ocean dynamics in the southern MAB, near Cape Hatteras. In July 1993, hydrographic data, and information on chlorophyll distributions, on continental shelf north of Cape Hatteras and across the shelf break at Cape Hatteras, showed a chlorophyll rich-bottom layer beneath the seasonal pycnocline characteristic of MAB cold pool; where constant density of chlorophyll rich waters, 25.0-to-25.6 sigma, along with a strong gradient along the 25 sigma isopycnals at the shelf break indicated MAB cold pool chlorophyll advection off the shelf at Cape Hatteras (Wood et al., 1996). The shipboard Ocean Margins Program in 1997 conducted a depth-resolved biogeochemical process study in the southern MAB, observing regions of seasonal productivity and chlorophyll, peaking on the shelf-slope front in spring and in subsurface high-nutrient intrusions on the shelf associated with the GS in summer (Lohrenz et al., 2002). And in August 2004 as part of a 7 day cruise, MAB cold pool waters were observed carrying chlorophyll rich water southward over the slope and outer shelf as part of shelf break jet, then shunted eastward and entrained into the GS (Churchill and Gawarkiewicz, 2014). These results build our insights to the distributions of chlorophyll as it relates to features of ocean circulation in the southern

proportion of the MAB. However, the studies only have a seasonally biased and a small temporal window of observations from several cruises in spring and summer to represent this physically highly complex system abutting several oceanographic regimes. To build on these results emphasizing the integrated bio-geophysical dynamics on the continental shelf, Fabry et al. (2008) recommended synthesis of data relevant to constraining the regional carbon budgets and cycling for the North American coastal continental shelf. Using a multiyear, seasonally resolved integrative approach on a broad spatial scale, with remote and autonomous measurements in the MAB, a study identified two major periods of enhanced chlorophyll biomass in fall-winter and spring, with the largest annual peaks occurring in the winter and the frequency of storms regulating the magnitude of the winter bloom and its light limitation (Xu et al., 2011). However, these multiyear findings, although integrative, are based on depth-resolved observations from a single cross shelf glider transect in the central MAB, off the New Jersey Coast, and surface remote sensing of the region. Hence, they do not sufficiently constrain or apply to fine scale chlorophyll dynamics in the southern MAB. Although studies are biased spatially or seasonally, they affirm the importance of seasonal, spatial, and depth resolved observations to consider metrics of southern MAB phytoplankton biomass distributions.

This study focuses on synthesis of data examining fine scale seasonal and inter-annual variability in the spatial distributions of chlorophyll associated with phytoplankton, the level of particulate organic carbon on the shelf in the southern MAB, and ultimately the exchange of carbon with the open ocean. To accomplish this considering the limited spatiotemporal observational coverage, we leverage high-resolution data collected during a recent observational program, the NSF-funded *`Processes driving Exchange At Cape Hatteras'* (PEACH), in the domain of the southern Mid-Atlantic Bight (Figure 2; Seim et al., 2022). This data was collected

by autonomous Spray gliders which are buoyancy driver vehicles moving along controlled paths. The biogeochemical glider data collected as part of the PEACH program provides the high spatial and temporal resolution chlorophyll fluorescence (fChl) observations necessary to derive seasonally resolved estimates of chlorophyll distributions in the southern MAB, described in data section 2.1. In data section 2.2, we describe the Ocean Color Standard set we use in our vicarious calibration of PEACH-fChl; and in section 2.3, we describe the independent *in situ* chlorophyll data we use to validate our calibration. In the methods section 3.1, we describe the implementation and validation of error offsets and a vicarious cross-calibration of PEACH-fChl based on satellite ocean color as a standard. In methods section 3.2, we describe our annual and seasonal spatial analysis of PEACH-fChl distributions and specific events. In results section 4.1, we described the validation results of the PEACH-fChl calibration. In results section 4.2 with the calibrated PEACH-fChl, a multiyear PEACH-fChl mean and standard deviation was derived for the southern MAB region on annual and seasonal timeframes. In discussion section 5.1, we critique the methods and analysis of the PEACH-fChl by considering the uncertainty associated with the calibration, the spatial bias, and capacity of the PEACH-fChl to observe biogeochemical processes. In discussion section 5.2, the PEACH-fChl distributions are put into context of what has previously been published and what are the likely processes are driving the distributions. In conclusion section 6, we finalize how our calibrated PEACH-fChl information fits in context of known geospatial and seasonal hydrographic background and has implications for future work using more sophisticated handling of spatial uncertainty, dynamic analysis, numerical, and machine learning techniques.

CHAPTER 2

DATA

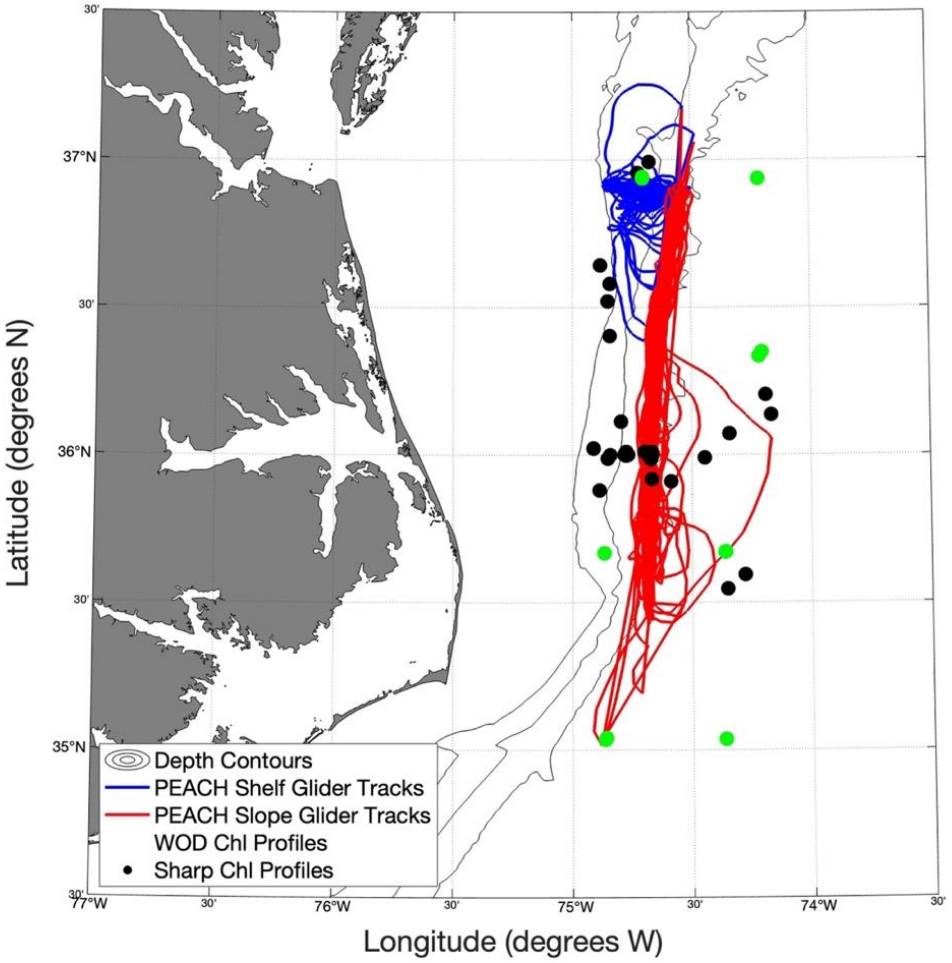

Figure 2. Map of southern MAB fChl observational coverage used in this study. Geographical distribution of Spray glider profiles collected of the course of the 2 year PEACH program, and the profiles available from the World Ocean Database (WOD, Black circles) and Sharp Cruise (Red circles). The PEACH program's repetitive glider occupations of slope and shelf transects, colored purple and orange respectively, are shown over and connecting the PEACH fChl

profiles. The blue-hued background contours show the depth of ocean (in m, color scale on the right).

2.1. THE PEACH SPRAY GLIDER FCHL DATA

Each PEACH Spray glider was equipped with a pumped Sea-Bird 41CP CTD, a 1-MHz Nortek AD2CP Doppler current profiler, and a Seapoint Chlorophyll Fluorometer (SCF). Each instrument received manufacture calibration immediately prior to deployment. From March 2017 to May 2019, the glider completed seven consecutive missions, traversing two specific transects: one along the upper continental slope (referred to as the slope transect in Figure 2, red), and one across the outer continental shelf (referred to as the shelf transect in Figure 2, blue). Table 1 presents geospatial and temporal resolution, as well as the extent of the resulting dataset. This dataset comprises 107 occupations of the slope transect, totaling 5042 profiles, and 73 occupations of the shelf transect, totaling 4128 profiles. The latitudinal and longitudinal boundaries for the slope and shelf transect are 74.91°W to 74.17°W, 35.01°N to 37.17°N and 74.87°W to 74.48°W, 36.39°N to 37.25°N, respectively. The glider trajectory starts southward along the slope for ~2°N at ~1500 m isobath for the slope occupation, then returns, proceeds westward onto shelf for ~0.5°W, across the shelf occupation, and back towards the slope to repeat the bimodal series. These occupations yield a temporal resolution of 1-to-14 days between occupations, ranging from immediate turnaround to ~2 weeks when returning from the longer slope transect (Todd, 2020a). The hydrographic data has been previously analyzed and published (Todd, 2020b).

The SCF employs blue light emitting diode lamps, commonly known as LEDs, which are modulated and further filtered blue with an excitation filter. This process directs photons at a specific spectrum to excite the chlorophyll sample. The resulting photons fluorescing from

chlorophyll are then filtered red, confirming only emission photons produced by chlorophyll are detected by the silicon photodiode, where the signal is captured. Subsequently, a synchronized demodulation circuit processes the weak signal, producing an output voltage that is proportional to the chlorophyll concentration in the water column (Seapoint, n.d.). The glider SCFs of the PEACH program (PEACH-fChl) were calibrated to chlorophyll concentration in mg m^{-3} using Seapoint Sensor, Inc.'s manufacture calibration before deployment. Previous studies of chlorophyll distributions in this region have reported strong statistical relationship between chlorophyll concentration determined from analysis of water samples, between 35.3°N and 36.4°N over the Hatteras shelf and slope, and *in situ* fluorescence signal of fluorometer, finding a linear relationship of $R^2 = 0.906$ (Wood et al., 1996). However, the chlorophyll concentrations estimated from chlorophyll fluorescence (fChl) measurements, such as PEACH-fChl, are subject to uncertainty due to calibration errors, sensor drift and biofouling (Palevsky et al., 2022). Ideally as best practice, underwater autonomous observations of fChl are regularly calibrated by shipboard sampling of chlorophyll, however this limits the autonomous capacity of the observations. In this study, no concurrent shipboard observations of chlorophyll were collected concomitantly during the 2 year glider deployment. Therefore, a vicarious calibration method for standardizing PEACH-fChl using remote sensing ocean color data was developed and applied. This standardization is an expansion of previous studies targeting autonomous fChl sensor data best practices to correct for known sources of uncertainty and error (Boss et. al. 2008, Lavigne et. al. 2012). The vicarious calibration process, which will be described in detail in section 3.1, involves a robust regression to derive remote sensing multiplicative gain standard correction factors, accompanied by correction of offset errors and validation using independent chlorophyll datasets from the study region.

Table 1. PEACH Spray Glider Data Information.

	Number of Occupations	Number of profiles	Approximate Geospatial Length	Temporal Resolution (occupation-to-occupation)	Temporal Resolution (Dive-to-dive)	Geospatial Resolution (Dive-to-dive)	Latitudinal Bounds	Longitudinal Bounds
Slope Transect	107	5042	~2°N	~8 days	~3 hrs.	2 km	35.01°N to 37.17°N	74.91° W to 74.17° W
Shelf Transect	73	4128	~0.5°W	1-to-14 days	~1 hr.	~200 m	36.39°N to 37.25°N	74.87° W to 74.48° W

2.2. OCEAN COLOR STANDARD DATA

Since there are no concomitant shipboard observations to the PEACH-fChl dataset, we rely on remote sensing ocean color (OC) to act as standard values of chlorophyll across all the PEACH-fChl glider missions. While using OC data for calibrating fChl from autonomous platforms can be subject to higher uncertainty than when using coincident chlorophyll data generated by HPLC or other standard lab methods, previous research has demonstrated this standardization approach to be accurate to the extent of the uncertainty associated with the OC instrument (Lavigne et al., 2012). In this study, the concomitant standards are VIIRS L-2 OC pixels which are at a resolution of 750m (NASA Ocean Biology Processing Group, 2017), an increase from resolution by Lavigne et al. where MODIS OC was used. These concomitant pixels are extracted from daily swaths, providing data coincident with the PEACH-fChl profiles. To avoid errors that might be introduced as a result of fluorescence quenching during the day, only nighttime fChl profiles were utilized in the calibration. However, it is important to note

this approach may introduce a spatial discrepancy due to temporal lags in a physically dynamic system. Previous studies performing matchups have overcome this by using temporal windows of ± 3 hrs. from noon when the swath passes over (Bailey and Werdell, 2006). While, due to quenching concerns, this study defines the temporal window to ± 12-hrs. Upon that established context, the large standardization sample size (n = 5,174) of concomitant OC pixel matchups to PEACH-fChl limits potential error to only the two sources of uncertainty: the temporal lag of the matchup and the OC instrument's uncertainty.

Even though we continue to handle and acknowledge the uncertainties of the OC standardization, every step of resolution refinement and validation is important because previous work acknowledges chlorophyll variability is associated with meso-to-submeso scales (10-to-100 km) driven by ocean dynamics (Churchill and Gawarkiewicz, 2014) and isolated regions of productivity (Lohrenz et al., 2002). This acknowledgement of uncertainty is most important when interpreting the scale of the mean and specific events. Notably the intra-relative distribution and relationships, that is the relationships standing within the scope of the PEACH-fChl set, that are derived from the standardized PEACH-fChl are safe from this potential "standardized error" from OC uncertainty. However, for the goal of comparing these results with those of other studies in terms of relative magnitudes of chlorophyll, the potential for standardized error is the motivation for the inclusion of the following independent *in situ* regional fChl validation set in our analysis.

2.3. REGIONAL *IN SITU* FCHL VALIDATION SET

In addition to the OC standard described above, we employed an additional independent fChl validation as a key component of this study to provide confidence in the calibrated PEACH-fChl data. The regional independent validation relies on two additional *in situ* datasets: the

World Ocean Database (WOD; Boyer et al., 2018), and data collected in the study region on the R/V Sharp Cruise (Sharp) provided by Dr. Margaret Mulholland's Lab at ODU. The regional independent validation data was bounded by the geographic extremes (74.91°W-to -74.17°W, 35.01°N to 37.17°N) of the slope occupation *(see section 2.1)*.

The WOD is a publicly available database that contains a wealth of oceanographic data, including fChl profiles in the study domain sparsely between the years from 1969 to 2019. The Sharp sampling consisted of eight cross shelf transects aboard the R/V Hugh R. Sharp in August 2016. Sharp data from only four of the transects are used here due to the bounds of our study domain (Figure 2; Selden et al., 2021). In these transects, fChl was measured using an ECO AFL/FL WET Labs chlorophyll fluorometer and was calibrated immediately prior to sampling by the technician onboard. Data access methods are described in the supplementary material. The independent data included 44 WOD- and 11 Sharp- fChl profiles within the geographical extremes of the slope occupation portion of the PEACH study region (Figure 2).

CHAPTER 3

METHODS

3.1. FOUR PART VICARIOUS CALIBRATION

To handle the various potential sources of error in estimating chlorophyll concentration using PEACH-fChl described above in section 2.1, the following methods are implemented to enhance our confidence in cross-mission analysis. All reference to PEACH-fChl after section 3.1 will refer to the fully calibrated PEACH-fChl dataset. Various values from the mission offset and standardization are included in Supplementary Table 1.

3.1.1. DARK OFFSET CORRECTION

A dark offset, in essence, is an offset to a known zero at depths where light does not penetrate and chlorophyll does not exist, below the euphotic zone. This offset addresses errors on short spatial intervals, by application on a profile-by-profile basis.

In this study, the dark offset correction is applied by subtracting the minimum value of each fChl profile from the corresponding profile fChl data at all depths, using the equation (2), in units of fChl, chlorophyll concentration in mg m^{-3}. Instead of using all values greater than a depth-threshold for complete darkness, the minimum value was chosen. We then verified these minimum values where below the euphotic zone, by being at deeper than the 1% isolume, $z_{1\%}$, The 1% isolume was calculated with equation (1), using kd_{490}, VIIRS remote sensing attenuation coefficient and deriving the relationship from first principles (Morel et al., 1988).

$$z_{1\%} = -\log(0.01) / kd_{490} \quad (1)$$

By applying the equation 2 below to every PEACH-fChl profile, known zeros visually associated with non-zero minimums at depth in the raw profiles were adjusted to zero, effectively eliminating artifacts caused by unrealistic values of chlorophyll at depth.

$$fChl_{corrected} = fChl_{uncorrected} - fChl_{min} \quad (2)$$

Where the $fChl_{uncorrected}$ is the uncalibrated PEACH-fChl with no offsets or corrections applied; the $fChl_{corrected}$ is the output corrected PEACH-fChl after dark offset is applied; and $fChl_{min}$ is the minimum value of each chlorophyll profile, verified to be below the 1% isolume.

Both independent *in situ* validation datasets included uncorrected fChl profiles, identified due to the presence of unrealistically high values of chlorophyll at depth, down to 1000 m prior to the offset. Therefore prior to our comparison, we applied the same dark offset that we applied to the PEACH-fChl to all independent dataset profiles.

3.1.2. EXPONENTIAL DECAY OFFSET

Exponential offsets are used to account for sensor drift that occurs over time from the initial manufacture calibration because of factors such as aging of the sensor's semiconductor components, environmental factors, contamination, mechanical stress, and electrical factors; which produce a decay in the signal over time. To account for the potential drift of each instrument in the series of PEACH-fChl glider missions, the final offset ($offset_f$ in fChl mg m^3) is obtained by applying the exponential decay offsets ($offset_{data}$) as function of time (t) over the entire mission as:

$$offset_f = offset_{data} + a_0 e^{-\frac{t}{T}} \quad (3)$$

$$fChl_{corrected} = fChl_{drift} - offset_f \quad (4)$$

where in equation (3) a_0 is the amplitude of the offset (mg Chl m^{-3}) and T is the time scale (seconds) of offset and equation (4) the $fChl_{drift}$ is the PEACH-fChl before the exponential offset is applied and $fChl_{corrected}$ is the PEACH-fChl after being corrected for potential sensor drift.

3.1.3. OCEAN COLOR REMOTE SENSING STANDARD CALIBRATION

Remotely sensed OC is used as a concomitant standard for the calibration of PEACH-fChl, in lieu of *in situ* chlorophyll measurements. The regression techniques used to establish the concomitant standard calibration are described as follows.

Linear regression of the space-time matchup of PEACH-fChl profiles with standard OC pixels was used to derive a multiplicative correction factor for each glider mission, or gain: a ratio of outputted standardized PEACH-fChl signal to the input uncorrected PEACH-fChl signal. The linear fits were forced through the zero intercept to isolate the standardization to only one multiplicative term. Each PEACH-fChl profile is matched with the surface OC pixel on the same day and in the same location, using the temporal window described in section 2.2. Therefore, the uncalibrated input glider PEACH-fChl profiles must be averaged to only one value of what is observable by the OC instrument to develop a representative regression model. To accomplish this, a depth-weighted mean of PEACH-fChl profiles within the first optical depth, the portion of the water column that contributes to the reflectance signal received by the VIIRS radiometer, is calculated for each of the PEACH fChl profiles. The optical depth mean PEACH-fChl is estimated by calculating the logarithmically weighted average of the PEACH-fChl to the optical depth of the OC instrument derived from the light attenuation coefficient at a wavelength where

chlorophyll absorbs light, Kd490. The 10% isolume is used as the optical depth and all fChl observations below that depth are excluded in the logarithmically weighted average. In principle, this represents 99% of the optical field that contributes to OC reflectance values, derived from first principles that surface OC reflectance is constrained by logarithmic attenuation over the vertical optical field as function of pathlength (Zaneveld et al., 2005). To logarithmically weight the profile, all values beyond the 10% isolume were excluded out and all values above were weighted using:

$$z_{od\_OC} = -\log(0.1)\,/\mathrm{kd}_{490} \tag{5}$$

$$fChl_{ow} = fChl * (-\log(\frac{z_{fChl}}{z_{od\_OC}}) \tag{6}$$

Where *fChl* is PEACH-fChl from each profile in units of chlorophyll concentration in mg m^{-3}, $fChl_{ow}$ that will be incorporated into the regressions, z_{fChl} is the depth of the PEACH-fChl measurement that is being weighted, and z_{od_OC} is the optical depth of the OC reflectance measurement, described above, in meters.

The outliers, in populations of both the condensed PEACH-fChl input and OC standard, influenced the regressions; therefore, outliers greater than 3 standard deviations from the mean of respective mission were identified and removed prior to fitting the regressions. Once the multiplicative gains were established using the tailored regressions described above, they are applied using equation 7, below, to obtain the fully calibrated PEACH-fChl for each of the individual glider missions as:

$$fChl_{standardized} = gain * fChl_{unstandardized} \quad (7)$$

Where fChl is in units of chlorophyll concentration in mg m^{-3} and the gain factor is in units of delta(OC)/delta(PEACH-fChl) from the slope of the fitted regressions described above.

3.1.4. EVALUATION OF THE PERFORMANCE OF THE OC VICARIOUS CALIBRATION

Two methods were implemented to validate the results of the vicarious PEACH-fChl calibration described above. First, the reduction of cross-mission variability as a result of the calibration was assessed. Quantifying the reduction of cross-mission variability checks for improved cross mission comparability and relative precision. Second, the calibrated PEACH-fChl was compared to independent regional *in situ* fChl measurements to assess how well the data agreed. As the validation data were not collected concurrently with the PEACH-fChl data, and spanned several years prior to the PEACH program, the data were compared over the entire study region on a monthly mean basis. Comparing the independent, calibrated *in situ* observations verifies absolute accuracy.

3.1.4.1. QUANTIFICATION OF THE REDUCTION OF CROSS-MISSION VARIABILITY

Reducing cross-mission variability supports the interpretation of PEACH-fChl across missions by quantifying the reduction of systematic variability between missions that would make cross-mission differences due to mission specific calibration uncertainty. An output product with reduced cross mission variability is more comparable and precise across the entire multi-mission PEACH program. The reduction of PEACH-fChl cross-mission variability was quantified by computing the standard deviation between individual mission means normalized by

the mean of all the PEACH-fChl values before and after the corrections were applied. This approach wholistically quantifies the difference between before and after calibration, in the array of individual PEACH glider mission fChl means. The normalization by the overall mean is necessary because the individual applied gains can either increase or decrease the variability of individual missions, while all gains together reduce variability across the entire multi-mission dataset. The normalized mission mean was obtained by normalizing each mission mean by the mean of the entire suite of missions. The normalized mission means described above are computed with the equation below,

$$\bar{x}_{normalized\ mission} = \left|\left(\frac{\bar{x}_{mission}}{\bar{x}_{data}}\right) - 1\right| \quad (8)$$

where $\bar{x}_{mission}$ is the mean PEACH-fChl from one glider mission, $\bar{x}_{data}$is the average value of PEACH-fChl from all glider missions, and $\bar{x}_{normalized\ mission}$ is the normalized mission mean output. Once, the normalized mission means have been computed before and after the calibration, the standard deviation of these sets is compared.

3.1.4.2. VALIDATION OF PEACH-FCHL WITH INDEPENDENT REGIONAL *IN SITU* DATA

To assess how well the OC-calibrated PEACH-fChl corresponds to previously observed chlorophyll profiles in the study region, we compared monthly mean PEACH-fChl profiles to fChl profiles obtained from WOD (all months except January and December) and Sharp (August).

3.2. SPATIAL AND SEASONAL ANALYSIS OF PEACH-FCHL

3.2.1. SEASONAL SEPARATION

The two years of glider data are separated into different seasons based on mixed layer depth (MLD) and PEACH-fChl dynamics using two sets of student t-tests. Seasonal groups were bounded to identify seasonal chlorophyll dynamics in this region occurring before and after the onset of stratification. This approach expands on descriptions by Lohrenz et al. (2002). These two seasonal identifiers were analyzed with yearday-means of MLD and depth integrated chlorophyll. Once, analyzed groups were visually separated based on the apparent transitions in yearday means of MLD and depth integrated PEACH-fChl, then these groups were tested for their significance with the student t-test. Yearday-mean MLD patterns were used to distinguish seasons of high and low stratification. We calculated the MLD of each profile based on a density threshold, where the MLD is determined to be the depth which potential density is 0.3 kg m^{-3} greater than at the reference density at the surface (de Boyer Montégut et al., 2004). Then, yearday-mean depth integrated PEACH-fChl patterns were grouped to distinguish seasons of high and low chlorophyll into two groups from already significant the high MLD group. This grouped the two seasons outside of the stratified summer season, winter-spring and fall. The depth integrated PEACH-fChl ($fChl_{DI}$, in units of mg chlorophyll m^{-2}) was calculated as:

$$fChl_{DI} = \sum_{n=i}^{z}[(fChl_i + fChl_{i+1})/2] * (z_i - z_{i+1}) \quad (9)$$

Where the integration was done over the total number of observations (n) in each profile over the entire depth (z) of the water column.

3.2.2. SPATIAL BIN CALCULATION OF PEACH-FCHL MEAN AND STANDARD DEVIATION

The mean and standard deviation distributions of PEACH fChl, temperature, salinity, and potential density were obtained by binned calculations over geographic degrees in the horizontal plane and meters depth in the vertical plane. Previous analyses of the PEACH Spray glider dataset indicated that averaging the data over 0.10° and 0.25° resolution of longitude and latitude for the shelf and slope respectively, is adequate to resolve features and may average out potential sources of spatial uncertainty from using these moving platforms (Todd, 2020a). The vertical resolution was retained at 10 m, the original vertical resolution of the processed PEACH glider data product.

The temperature and salinity outputs of spatially binned means were compared with the results of Todd (2020a) that were obtained with a more sophisticated variability weighting to assess the differences. For context, Todd (2020a) produced mean distributions output grids of temperature and salinity with 5 km and 1 km spacing for the slope and shelf, respectively.[27] These distributions were derived using a weighted least squares regression, with a broad scale horizontal variability filter of approximately 25 and 10 km for the slope and shelf respectively, to account for sources of internal variability from using a moving platform, the Spray glider. Alternatively, in these spatial bins, we utilized resolutions that exceed the scales of internal variability established in Todd (2020a) to help mitigate the sources of internal variability. For context 0.01° of latitude and longitude is greater than 1 km at this latitude.

To prevent biases stemming from averaging over a relatively small number of observations in this highly variable system, we refined regions of the domain to exclude spatial bias and regions where the minimum number of observations was below a given threshold were removed;

yielding 3 and 5 horizontal bins from 74.8 to 74.6°W and 35.75 to 36.75°N on the shelf and slope transects respectively. Spatial bins that contained fewer than 10% of maximum number observations per bin were excluded from the analysis, resulting in an effective threshold 184 profiles per bin to be included in the spatial averaging. Once the spatial domain was sufficient vetted, the method of spatial bin calculation was then applied to the complete PEACH dataset generating the annual distributions and subsets of PEACH dataset derived from the results of the determined seasonal groups generating seasonal distributions.

Due to a lower number of observations in each seasonal subset from the method described above, section 3.2.1, the threshold of a minimum number of observations was not applied for each seasonal mean and standard deviation. Rather all available observations were used to compute the multiyear seasonal mean and standard deviation distributions in the same refined study domain used for the multiyear annual distributions. Consequently, the seasonally subsampled spatial calculations of the multiyear seasonal distributions may be influenced by larger spatial biases than the multiyear annual distributions (see Supplementary Figures 3 and 4).

3.2.3. IDENTIFICATION OF DEEP CHLOROPHYLL EVENTS

To identify chlorophyll at depth, the PEACH-fChl dataset was searched for profiles with chlorophyll concentrations that contained observations that met thresholds of: > 100 m depth and > 0.75 mg m^{-3} PEACH-fChl. Typical chlorophyll values after the dark offset should be close to zero due to light limitation below 100m; beyond ~90 m, the mean value plus one standard deviation of all 1% isolume values in refined study domain used to calculate spatial distributions of PEACH-fChl. Beyond this depth, there will be only a few nonzero PEACH-fChl exceptions associated with deviations from euphotic drivers of chlorophyll structure. Furthermore, the 100 m depth criterion was chosen because it is greater than the maximum value of the yearday-mean

MLD, 84 m, suggesting that episodic physical dynamics are necessary to drive high concentrations of fChl from euphotic zone to depths greater than 100m. From those physical and euphotic constructs around the > 100 m threshold, observations greater than 0.75 mg m^{-3} fChl were then assumed to be associated with transport of chlorophyll-rich water to depth. Therefore, these profiles showing high chlorophyll at depth are distinguished, deep chlorophyll profiles. We then group the deep chlorophyll profiles into individual events, which in some cases included several deep chlorophyll profiles because consecutive profiles that were less than 3 days and 20 km apart in time and space, respectively, were grouped together.

Observations were then further characterized based on salinity characterizations from Todd (2020a) with < 34.5 PSU and > 36 PSU to distinguish MAB and GS water masses.[27] Profiles falling within this salinity range, contextualized as anything in between those two regimes, were considered possible exchange and mixing of those two regimes maybe occurring.

CHAPTER 4

RESULTS

4.1. CALIBRATED PEACH-FCHL VALIDATION

4.1.1. NORMALIZED MISSION MEANS

The standard deviation of normalized mission means was reduced from 0.40 to 0.23, in normalized dimensionless units. The mean ± the standard deviation of PEACH-fChl changed from 0.13 ± 0.31 to 0.18 ± 0.24 mg fChl m^{-3}, increasing the mean and decreasing the standard deviation. This result demonstrates a reduction in the cross-mission variance of PEACH-fChl after the data were calibrated using the OC standard. The series of normalized mission means retain a portion of the variability between missions before and after the correction which is likely due to the natural variability of chlorophyll in this system (Figure 3).

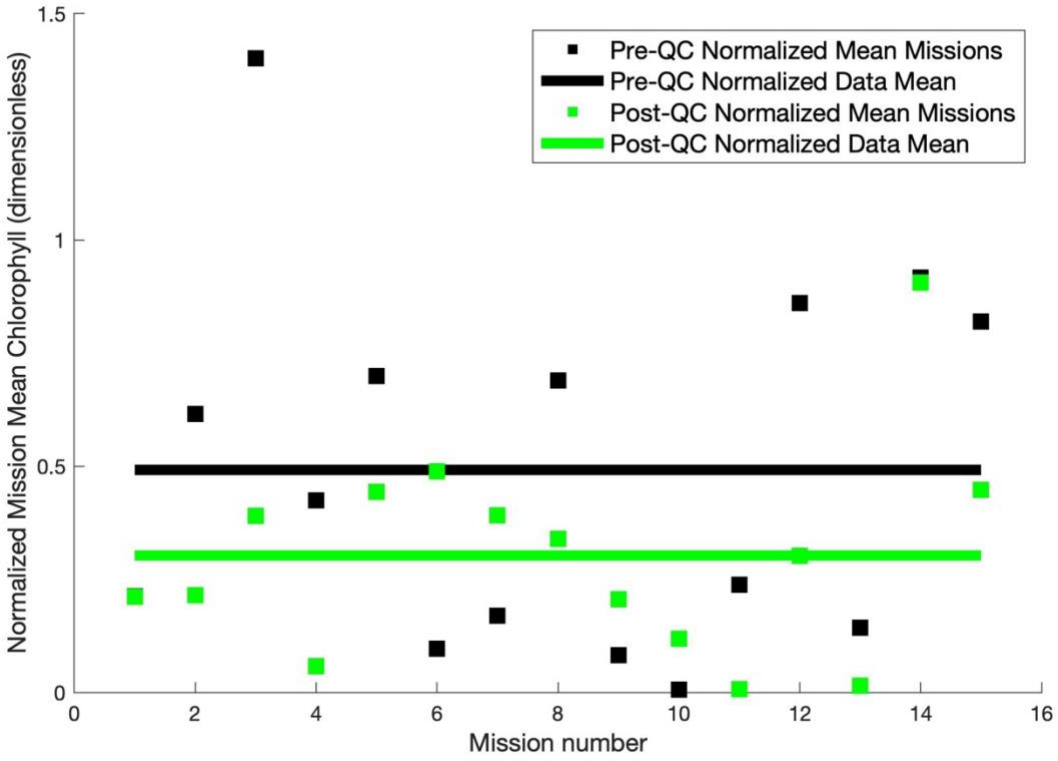

Figure 3. Normalized Mean of Missions before and after the Calibration of PEACH Spray gliders. The prep and post normalized data mean is the mean of those normalized mission means to show the change in scale of PEACH-fChl.

4.1.2. VALIDATION OF PEACH-FCHL WITH INDEPENDENT CHLOROPHYLL DATA

The PEACH-fChl was compared to *in situ* data derived from the Sharp cruise and WOD chlorophyll datasets from the study region to how well assess skill the OC calibration performed. Figure 4 shows the comparison of the monthly mean profiles of PEACH-fChl with *in situ* chlorophyll data.

All the monthly mean profiles generally have the same vertical structure, that shows chlorophyll maximums near the surface and slightly subsurface then decreasing concentration

with depth. The scale of their differences between PEACH-fChl and *in situ* monthly mean profiles is within the standard deviations, except for October (Figure 5G). The best agreement between PEACH-fChl and the WOD chlorophyll data is observed in the summer months, specifically in May through September (Figure 5B through F). The PEACH-fChl August data also agrees well with the Sharp mean profile over the top 80 m (Figure 5I). Poor agreement is only observed in a few of the mean fChl profiles of WOD during months with small sample populations (2 to 4 profiles; Figure 5A&G). The PEACH-fChl values consistently appear lower than those of *in situ*-fChl, except for September, suggesting that PEACH-fChl may slightly underestimate chlorophyll concentrations. However most importantly, the chlorophyll values are generally found within one standard deviation of each other, confirming that the PEACH-fChl data accurately represent realistic concentrations in the study domain.

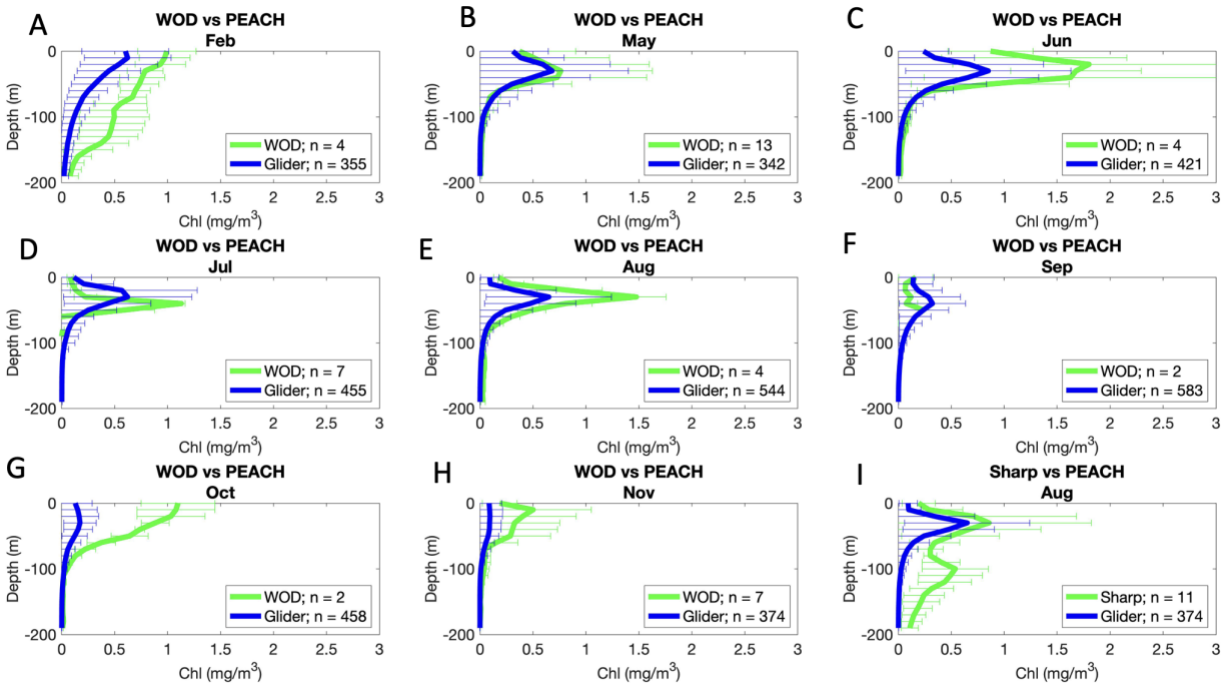

Figure 4. Monthly Mean fChl Profiles Comparison of the PEACH Spray Glider Chl. Seasonal-Month Mean Chl Profiles Comparison of the PEACH Spray Glider Chl to the two independent datasets, WOD and Sharp (Plots A through I). The error bars show the standard deviation of the profiles. The number of observations is included in the legend, n.

4.2. PEACH-FCHL DISTRIBUTIONS

The two years of PEACH-fChl observations used in this analysis show features that are consistent with the characteristic hydrography and biogeochemistry of the converging water masses in this study domain. Visualization of these fChl sections, as a function of geographic location and 10m depth bins, shows spatial and seasonal dynamics of chlorophyll and allows spatial association of these dynamics with known mean water mass features. For the rest of the results, there will be no more mention of the *in situ* fChl measurements from WOD and Sharp, and all references to fChl are interchangeable with PEACH-fChl.

4.2.1. FCHL ANNUAL MEAN AND STANDARD DEVIATION OF SLOPE AND SHELF TRANSECTS

The spatiotemporal bins are utilized to calculate the annual mean and standard deviation of the PEACH Spray glider slope and shelf transects, as explained in the subsequent subsections.

4.2.1.1. SLOPE FCHL ANNUAL MEAN AND STANDARD DEVIATION TRANSECTS

The two spatial distributions of the annual mean and standard deviation of PEACH-fChl for the slope transects is shown in Figure 5. The scale is from 0 to 1 mg m^{-3} fChl, with maxima in standard deviation and mean near the surface centering around ~20 to ~40 m in the northern half of the occupation, and the vertical minima found below depths of 150 to 250 m, across the transect. The system exhibits high variability, with relative standard deviations consistently exceeding the co-occurrent means. The relative magnitude of the standard deviation to the mean indicates typical fChl ranges on scale from complete absence of chlorophyll to greater than double the mean, which is diagnostic of reoccurring episodic and/or ephemeral phenomena.

The vertical structure of fChl exhibits a near surface maximum and thereafter the concentration of fChl decreases as a function of depth until the minimum at >150m (Figure 5). However, this vertical structure of chlorophyll is variable along the occupation. The near surface fChl maximum is relatively constant depth across the slope. However, the gradient of decreasing fChl as function of depth changes across the slope due horizontal southward trend of increasing fChl at depth. From the northern part of the occupation south to about 36°N, the decline in fChl roughly begins from 50 m down to ~150 m. Beginning at ~ 36°N, fChl values >0.01 mg m^{-3}, mean and standard deviation, increase depth from 150 to 250m at the southern end. This trend can be considered either as the decreasing gradient of chlorophyll as a function of depth or increase in both the mean and standard deviation of chlorophyll at depth of 150 to 200 m.

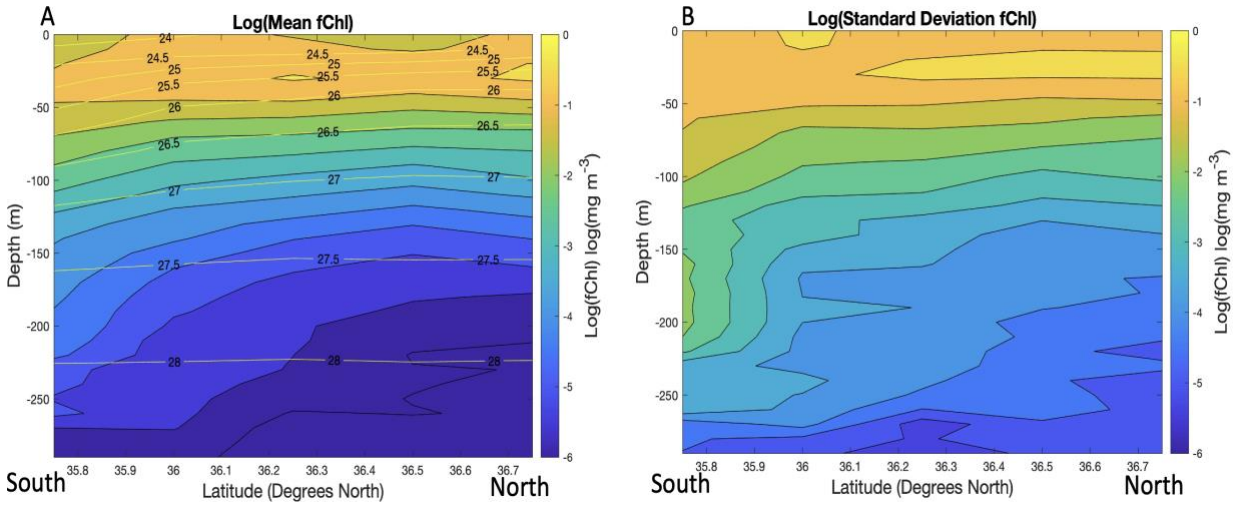

Figure 5. Slope fChl Annual Mean and Standard Deviation Transects. Spatially binned mean and standard deviations (left and right, A and B) of PEACH-fChl from the slope occupations as a function of depth and latitude. These are in 10 m depth by 0.35°W bins. The white contours are isopycnals of mean and standard deviation, left and right respectively, potential density in units of kg m^{-3}.

4.2.1.2. SHELF FCHL ANNUAL MEAN AND STANDARD DEVIATION TRANSECTS

The two spatial distributions of the annual mean and standard deviation of fChl on the shelf is shown in Figure 6. The scale is from 0 to 1 mg m^{-3} fChl. There is a subsurface maximum layer in both the mean and standard deviations of fChl at ~20-to-30 m depth, peaking shelfward in the mean (Figure 6A). The standard deviation maximum layer is vertically thicker towards the ocean/slope than the mean (Figure 7B). The fChl minimum mean and standard deviation occur at depths greater than 60m the near the shelf break.

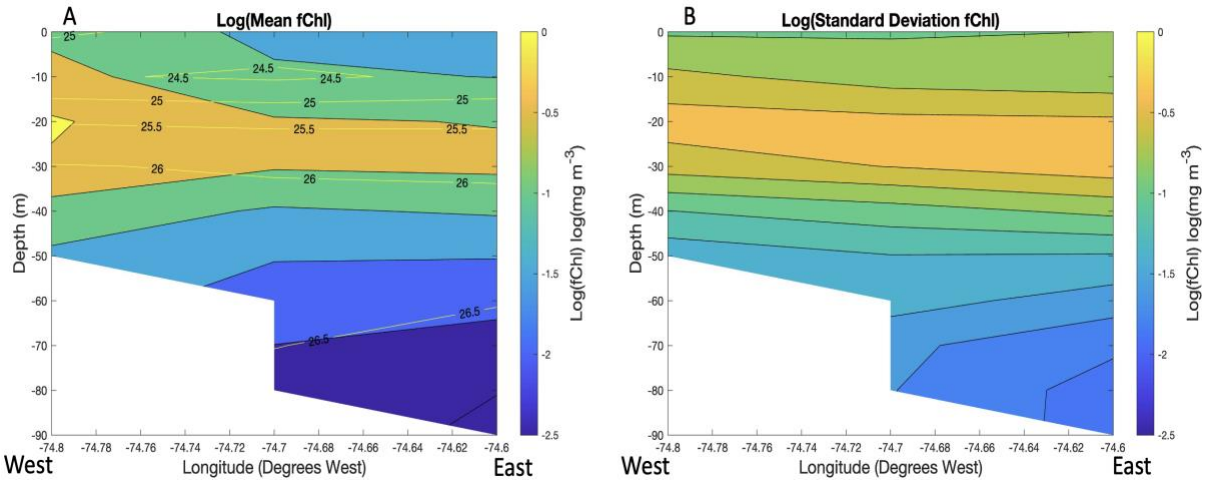

Figure 6. Shelf fChl Annual Mean and Standard Deviation Transects. Spatially binned mean and standard deviations (left and right, A and B) of PEACH-fChl from the shelf occupations as a function of depth and longitude. These are in 10 m depth by 0.1°W bins. The white contours are isopycnals of mean and standard deviation, left and right respectively, potential density in units of kg m^{-3}.

4.2.2. SEASONAL DISTRIBUTIONS OF FCHL

Three distinct seasons in the study region were identified based on two sets of t-test based on yearday-means of MLD and depth integrated fChl (Figure 7). The MLD yearday-means had relatively significant different group means (p-value<0.001): a low MLD group between yeardays 106 and 290 (summer), and a high MLD group which represented the rest of the year. The high MLD group was then further divided using a t-test based on the depth integrated fChl values, yielding a high fChl window between yeardays 1 and 106 (winter-spring), and a low fChl period between yeardays 290 and 365 (fall). The two periods differentiated by their depth-integrated chlorophyll values had relatively significantly different group means (p-value<0.001).

These results were used to define three seasonal windows: winter-spring, high MLD and high chlorophyll from yearday 1 to 106; and summer, low MLD between yearday 106 to 290; and a fall, high MLD and low chlorophyll yearday 290 to 365.

Using the seasonal windows defined above, the seasonal subset space bins are used to calculate the mean and standard deviation of both the PEACH Spray glider slope and shelf transects, which are described in the following sections.

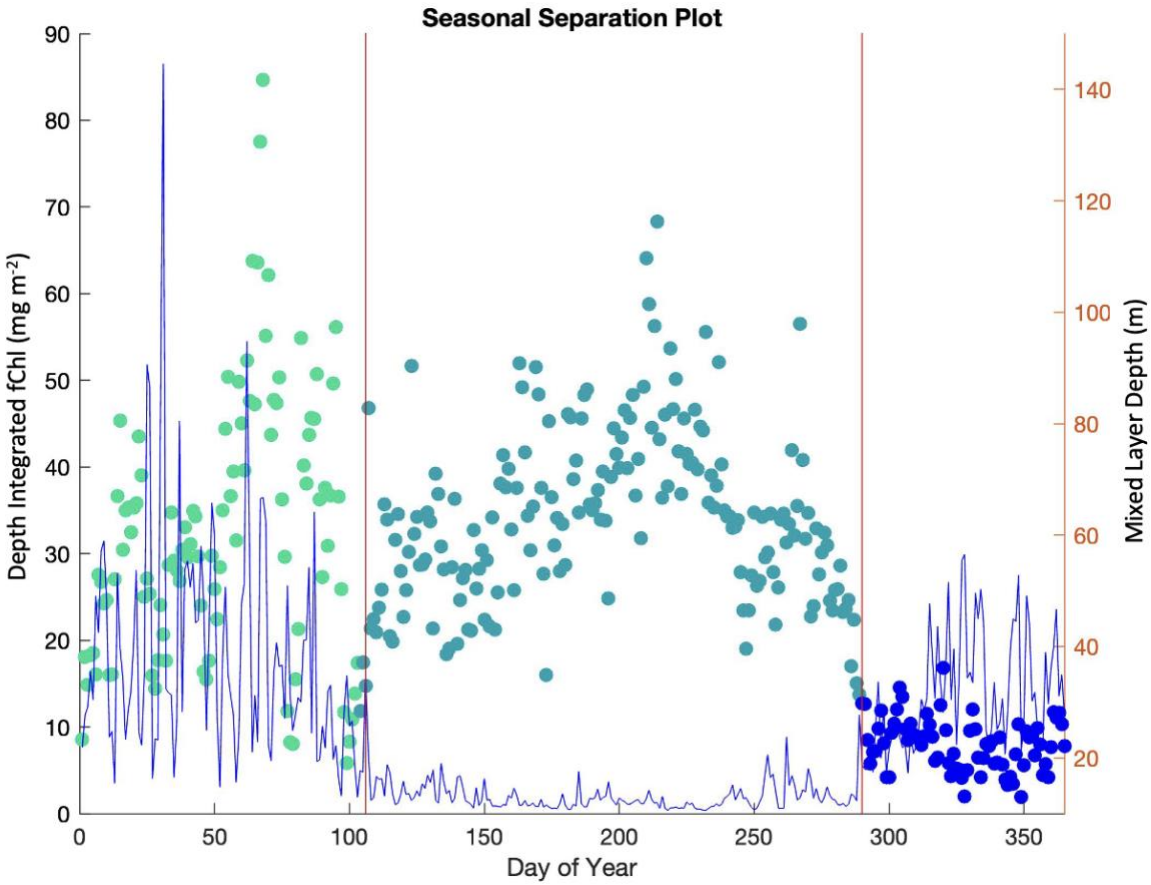

Figure 7. Seasonal Separation Series. The dots are all the yearday means of depth-integrated chlorophyll with associated scale on the lefthand axis. The line behind the dots is the yearday

Figure 7 continued.

means of Mix Layer Depth. Consecutive student t-test of the two parameters separated three seasons, separated by the vertical red lines on the plot, into Winter/Spring, Summer, and Fall.

4.2.2.1. SLOPE SEASONAL MEAN AND STANDARD DEVIATION TRANSECTS

The two spatial distributions of the seasonal mean and standard deviation of fChl for the slope transect in each of the three identified seasons, totaling six spatial distributions are shown in Figure 8. There are contrasts between seasons in the slope transects. The winter-spring season has the same depth distribution in both the mean and standard deviation of fChl as the annual mean and standard deviation (Figure 5). The point of difference (in Figure 8A and B) is the maximum of mean and standard deviation fChl is now from the surface to ~30 m where in the annual means this maximum is more subsurface (Figure 5). The summer season has the more pronounced subsurface fChl maximum in the mean and standard deviation (Figure 8C and D). There is no change in the maximum magnitude of mean and standard deviation fChl from season to season or season to annual, rather the latitudinal variability in the fChl depth distribution of winter-spring disappears in summer where the relative vertical structure of fChl is consistent along the transect. The combination of winter-spring and summer seasonal components are coherent with a timeseries decomposition of the annual distributions. While in the fall season, where depth integrated fChl was observed to be lower than in the other seasons, fChl is also much lower in the across the entire fall slope transects (Figure 8E and F), with values <0.1 mg m^{-3} fChl; suggesting the fall may only dilute the features of the other seasons in the annual slope distributions.

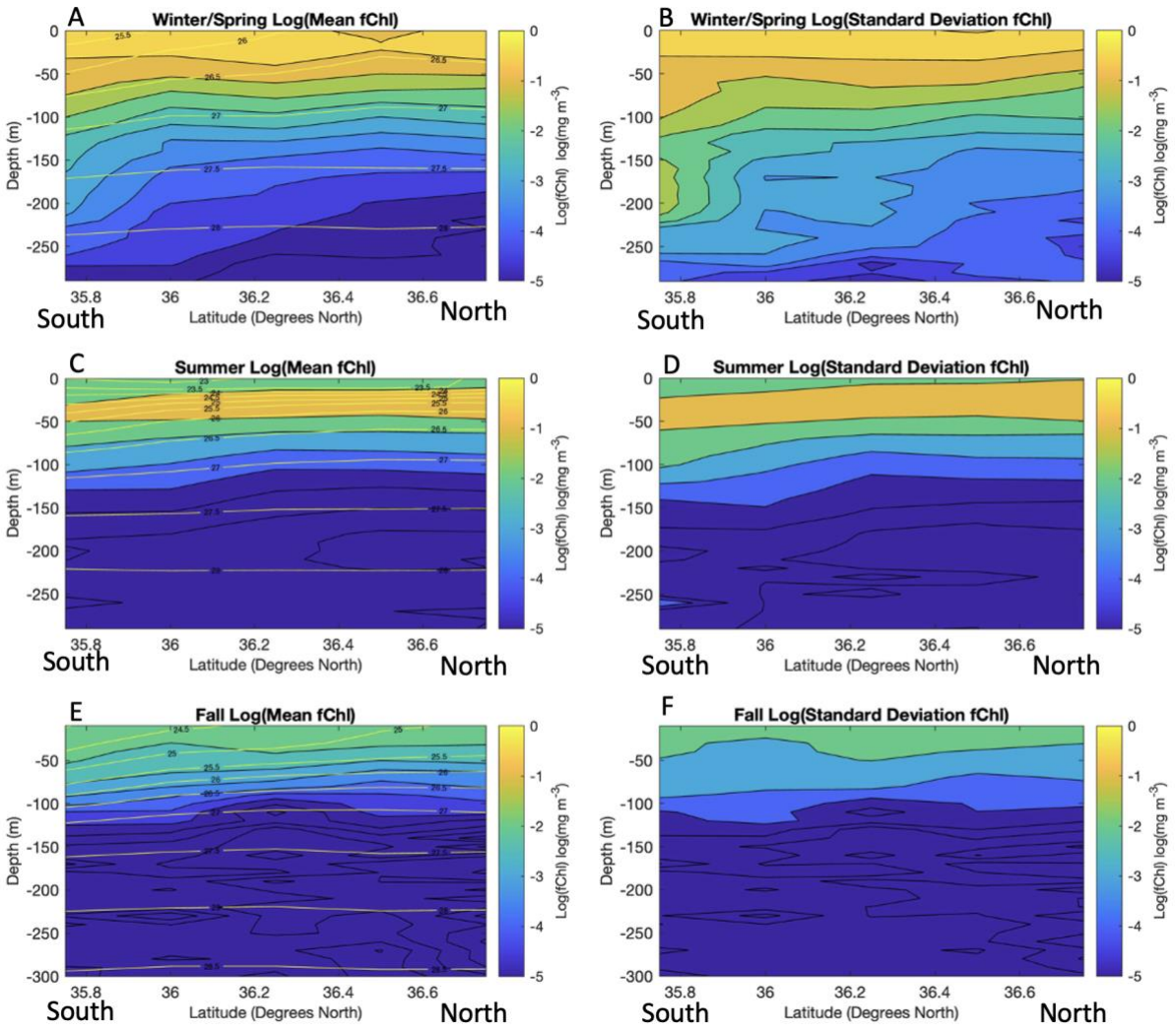

Figure 8. Slope fChl Seasonal Mean and Standard Deviation Transects. Spatially binned mean and standard deviations (in lefthand contour plots: A, C, and E; and in righthand contour plots: B, D, and F, respectively) of PEACH fChl from the slope occupations as a function of depth and latitude. These seasonal transects of the slope are derived from occupations of the slope confined in each seasonal subset from section 4.2.2, with seasons: winter-spring on top, summer in middle, and fall on bottom. These are in 10 m depth by 0.35°N bins. The white contours are isopycnals of mean and standard deviation, left and right respectively, potential density in units of kg m^{-3}.

4.2.2.2. SHELF SEASONAL MEAN AND STANDARD DEVIATION TRANSECTS

The two spatial distributions of the seasonal mean and standard deviation of fChl for the shelf transect in each of the three identified seasons, totaling six spatial distributions are shown in Figure 9. In the winter-spring season (Figure 9A and B), the vertical structure of mean and standard deviation of fChl was relatively constant to a depth of ~40 m, with a slight subsurface maximum observed in the mean and standard deviation, approximately 0.4 mg m^{-3} fChl, between 10m and 30m depth peaking on the shoreward end of the shelf transect. There is a subsurface maximum mean and standard deviation of fChl, at the same depths as winter-spring, across the shelf transect in the summer (Figure 9C and D), except this maximum is more pronounced relative to the surface and greater depths. In the mean, this more pronounced summer subsurface maximum fChl has greater magnitude on the shoreward end of the shelf transect, and the subsurface maximum in the mean is mirrored in the standard deviation, except slightly less pronounced in the vertical structure with no peak on the shoreward side. Coherent with the slope, the fall features the annual minimum standard deviation and mean fChl (Figure 9E and F). In fall, the mean value of fChl is higher on the shoreward end of the shelf transect from the surface to 50m, and standard deviation value of fChl is higher on the open ocean end of the shelf transect from the surface to 40m.

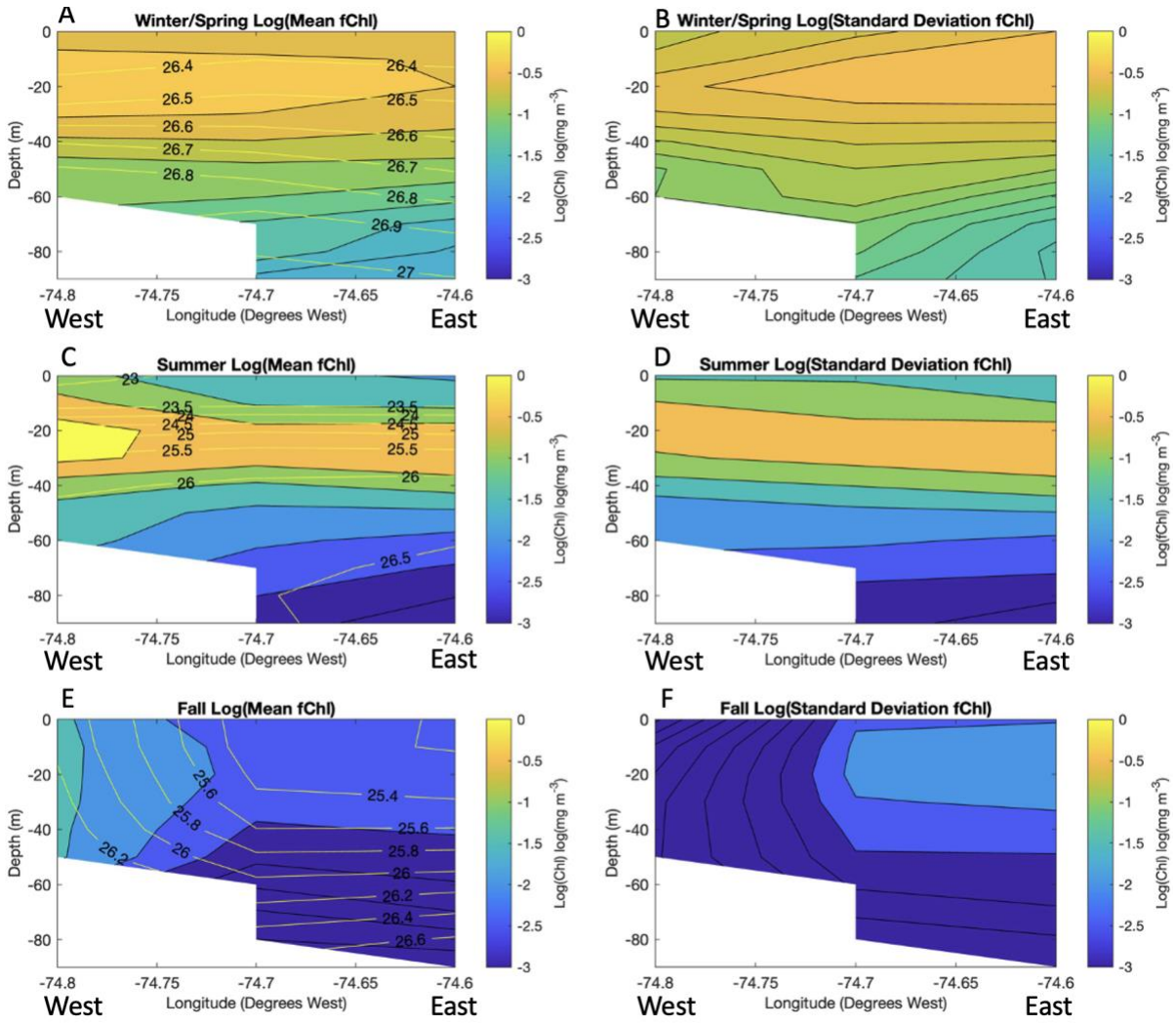

Figure 9. Shelf fChl Seasonal Mean and Standard Deviation Transects. Spatially binned mean and standard deviations (in lefthand contour plots: A, C, and E; and in righthand contour plots: B, D, and F, respectively) of PEACH fChl from the shelf occupations as a function of depth and longitude. These seasonal transects of the shelf are derived from occupations of the shelf confined in each seasonal subset from section 4.2.2. These are in 10 m depth by 0.1° W bins. The white contours are isopycnals of mean and standard deviation, left and right respectively, potential density in units of kg m^{-3}.

4.2.3. DEEP CHLOROPHYLL EVENTS IDENTIFIED IN SLOPE OCCUPATIONS.

Based on the thresholds defined to characterize deep chlorophyll, 69 profiles in 20 different occupations of the slope transect that contained values of fChl greater than 0.75 mg m^{-3} fChl at depths greater than 100m were identified. The mean yearday ± standard deviation for these deep chlorophyll profiles is 77 ± 49 and the median yearday for the events is 67, which is March 8th. Therefore, the seasonal distribution of these profiles is to the second half of the winter-spring season with several profiles in summer, in the months of June and July, skewing the distribution. The mean latitude ± standard deviation for these deep chlorophyll profiles is 35.97 ± 0.35 °N and the median latitude is 35.82°N; the along slope distribution is just north of the mean location of GS frontal wall (35.75°N) by ~0.07° latitude with several profiles skewing the distribution north. These skewed yearday and latitudinal deep chlorophyll profile distributions can be seen in histograms shown in Figure 10.

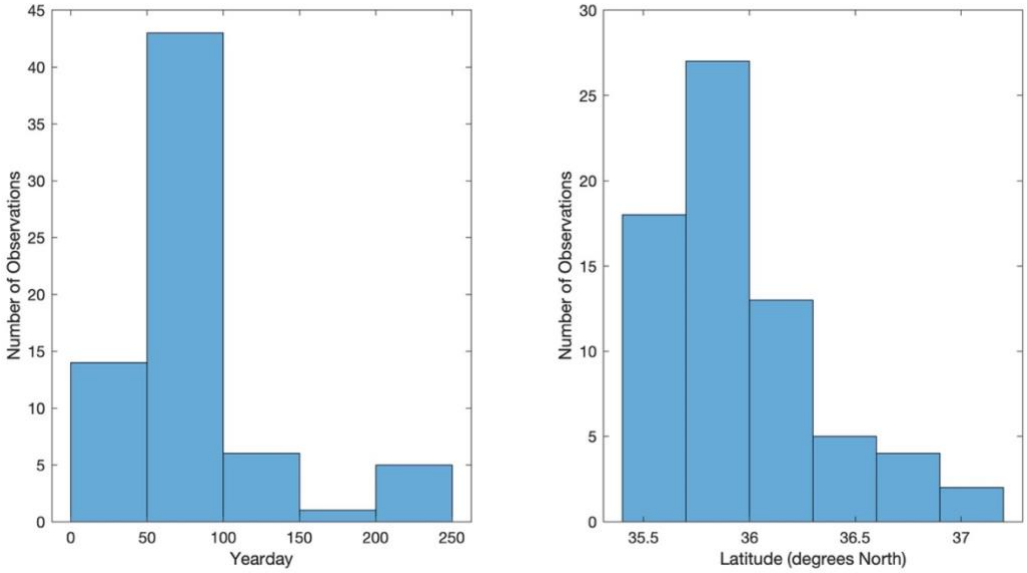

Figure 10. Deep fChl Event Profile Distribution. Histograms of the distribution of deep fChl profiles are shown to illustrate the median location and skew of these profiles in annually (in yeardays) and latitudinally (°N), respectively left and right.

In Figure 11 the deep chlorophyll observations are presented temperature-salinity diagram. The color scale ranges from 0 to 1.5 mg chlorophyll m^{-3} between 100 and 300 m. High chlorophyll concentrations exceeding 0.75 mg chlorophyll m^{-3} are represented as squares outlined in red, while additional PEACH-fChl observations with concentrations exceeding 0.3 mg chlorophyll m^{-3} are depicted as partially transparent circles. The boxes delineate the salinity domains of MAB shelf water and GS water, while the oval area highlights the potential zone of chlorophyll exchange between these geospatially adjacent water masses. The high deep chlorophyll concentrations, the squares outlined in red (Figure 11) are found along the 26.5 g kg^{-1} isopycnals on the fresher, cooler end of the oval area of possible exchange between

GS and shelf water. This isopycnal is denser than observed values warmer and saltier GS water and fresher shelf water containing chlorophyll in this depth range, suggesting chlorophyll only occurs in densest observations in these subsets.

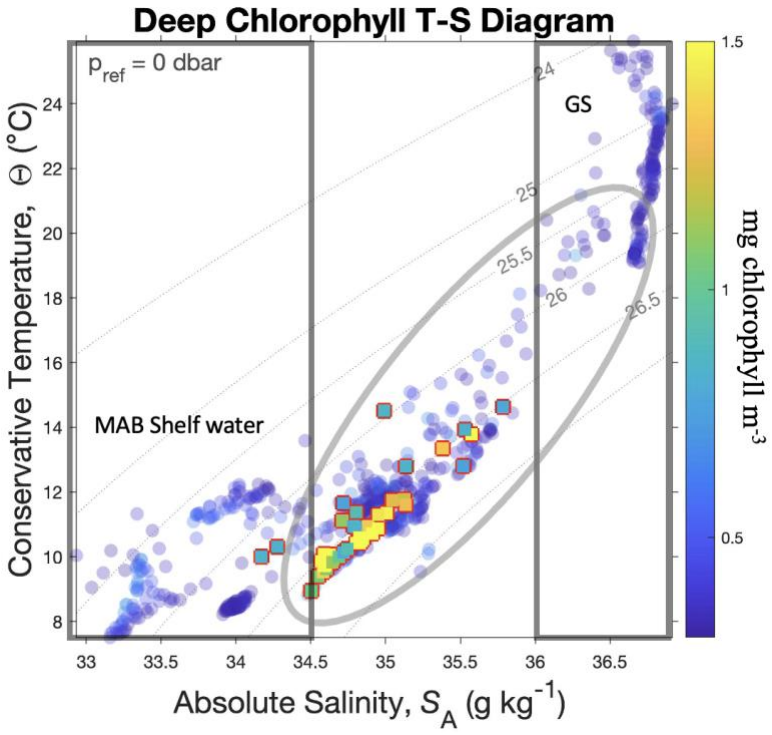

Figure 11. Deep Chlorophyll Temperature and Salinity Diagram. Above is a temperature-salinity diagram with concentration of chlorophyll in mg m^{-3} portrayed with a color scale from cool-to-warm for each of the points. The partially transparent circles are all the PEACH-fChl observations from the slope occupations from 100 to 300 m with greater than 0.3 mg chlorophyll m^{-3}. The squares outlined by a red border are all PEACH-fChl observations from the slope occupations from 100 to 300 m with greater than 0.75 mg chlorophyll m^{-3}, which meets the threshold for deep chlorophyll profiles described in section 3.2.3. The bottom left square distinguishes temperature-salinity values that are typical of shelf water and the top right square-

Figure 11 continued.

distinguishes temperature-salinity values that are typical of Gulf Stream (GS) water. The oval outlines the area where these two water masses could be exchanging chlorophyll.

From the 69 deep high chlorophyll profiles containing observations at >100 m with concentrations >0.75 mg m^{-3} fChl, 16 individual events were identified, based on the criteria that profiles less than 20 km or 3 days apart are considered to belong to the same individual event. From these 16 events, 10 have distinct vertical water mass features of relatively fresh (< 34.5 PSU), and cool (generally from 5 to 10 °C difference relative to the nearby GS, > 36 PSU) patches along isopycnals are showing coherence with the temperature-salinity diagram analysis above (Figure 11). Four representative examples of these 10 events are shown in white circled regions in Figures 12 through 15, each exhibiting distinct water mass patches visible in high fChl, cooler temperature, and fresher salinity. All these patches are directly adjacent to the GS frontal wall labeled by the red lines in Figures 12 through 15, which is associated with steeply sloped isopycnals roughly parallel to isotherms and isohalines. The patches are high fChl, fresher and cooler water extending to maximum depth of 237 m, underneath the GS. They differ in latitudinal width and distance underneath the GS; how far they extend to depth and how distinct the patches are across all the properties; and the steepness of the associated GS frontal wall. These events, 10 in the span of two years, potentially influence the multi-year and seasonal slope transect patterns of deep chlorophyll on the southern end of the transect.

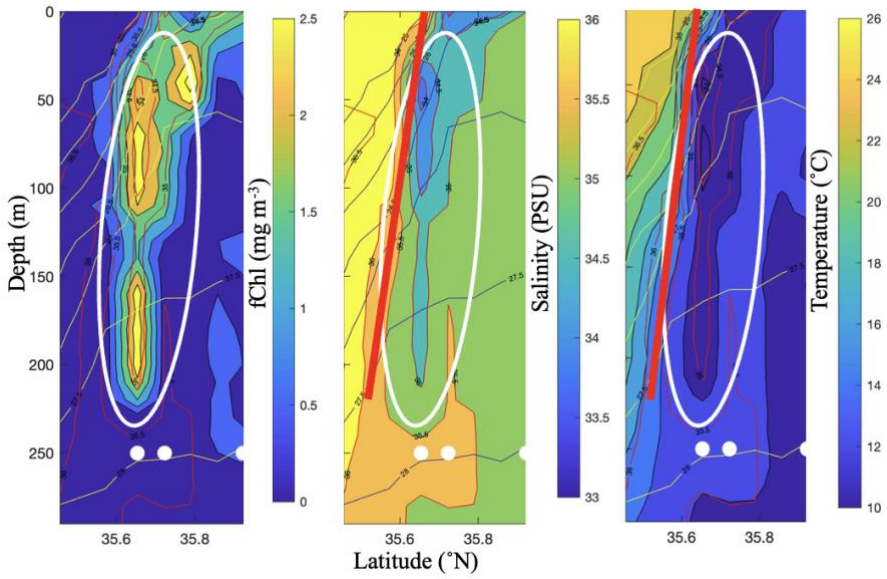

Figure 12. Characteristic Deep Chlorophyll Event identified on the Southern End of the Slope Transect in March 2017. Example one of the "deep chlorophyll events" from PEACH-fChl occurred in March 2017. These events were isolated from PEACH-fChl searching for values of 0.75 mg m^{-3} fChl beyond a depth threshold of 100 m. The three images across each event are 2-D distribution plots from the Spray glider occupation of the slope transect. Left to right the parameters are fChl in mg/m3, salinity in PSU, and temperature in °C with their associated color-bars directly right of the section. The vertical dimension is meters, seen on the far left. The white dots at 250 m depth are the latitudinal position of the deep chlorophyll profiles. The thin white (and black on the salinity plots) contour lines are isopycnals. The white circled region is a high chlorophyll, fresh and cool, water mass patch and the red line is the location of the Gulf Stream (GS) front with the GS to the south.

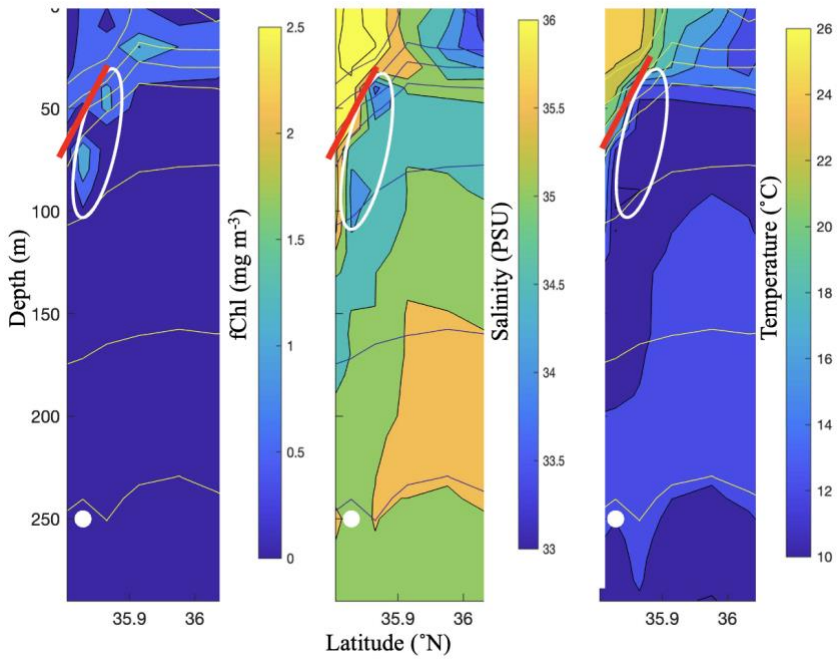

Figure 13. Characteristic Deep Chlorophyll Event identified on the Southern End of the Slope Transect in April 2017. Example two of the "deep chlorophyll events" from PEACH-fChl occurred in April 2017. These events were isolated from PEACH-fChl searching for values of 0.75 mg m^{-3} fChl beyond a depth threshold of 100 m. The three images across each event are 2-D distribution plots from the Spray glider occupation of the slope transect. Left to right the parameters are fChl in mg/m3, salinity in PSU, and temperature in °C with their associated color-bars directly right of the section. The vertical dimension is meters, seen on the far left. The white dots at 250 m depth are the latitudinal position of the deep chlorophyll profiles. The thin white (and black on the salinity plots) contour lines are isopycnals. The white circled region is a high chlorophyll, fresh and cool, water mass patch and the red line is the location of the Gulf Stream (GS) front with the GS to the south.

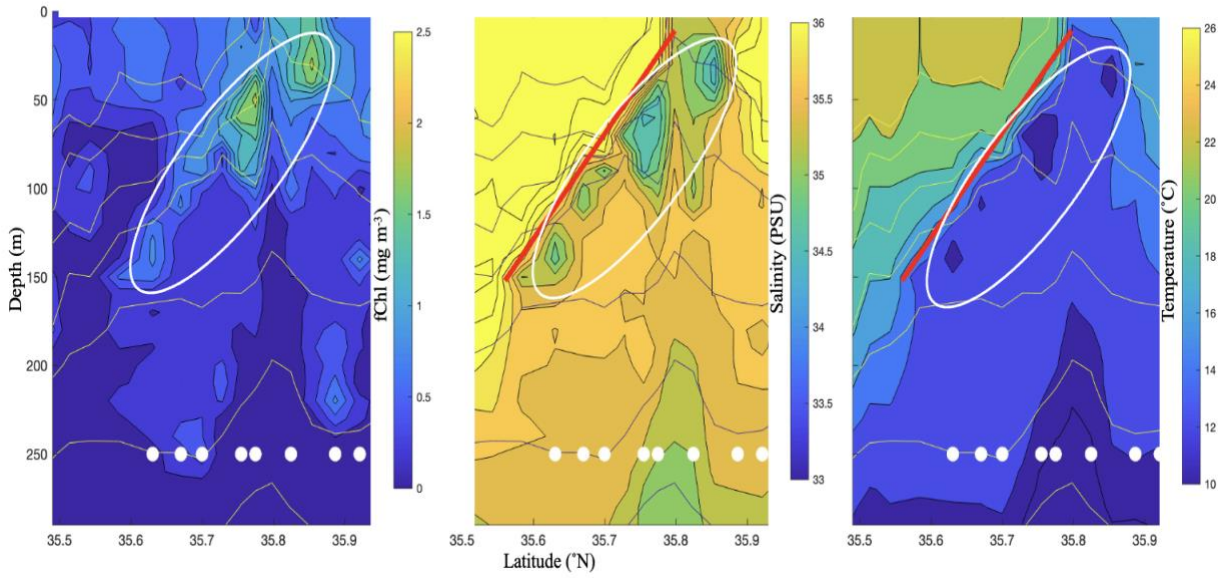

Figure 14. Characteristic Deep Chlorophyll Event identified on the Southern End of the Slope Transect in January 2018. Example three of the "deep chlorophyll events" from PEACH-fChl occurred in January 2018. These events were isolated from PEACH-fChl searching for values of 0.75 mg m^{-3} fChl beyond a depth threshold of 100 m. The three images across each event are 2-D distribution plots from the Spray glider occupation of the slope transect. Left to right the parameters are fChl in mg/m3, salinity in PSU, and temperature in °C with their associated color-bars directly right of the section. The vertical dimension is meters, seen on the far left. The white dots at 250 m depth are the latitudinal position of the deep chlorophyll profiles. The thin white (and black on the salinity plots) contour lines are isopycnals. The white circled region is a high chlorophyll, fresh and cool, water mass patch and the red line is the location of the Gulf Stream (GS) front with the GS to the south.

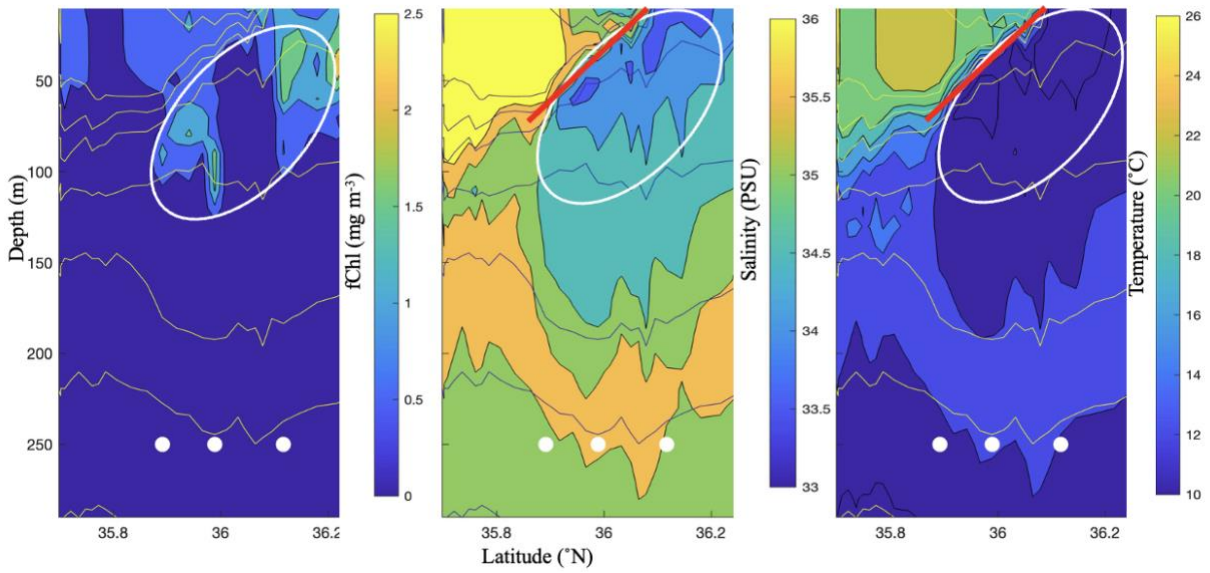

Figure 15. Characteristic Deep Chlorophyll Event identified on the Southern End of the Slope Transect in March 2019. Example four of the "deep chlorophyll events" from PEACH-fChl occurred in March 2019. These events were isolated from PEACH-fChl searching for values of 0.75 mg m^{-3} fChl beyond a depth threshold of 100 m. The three images across each event are 2-D distribution plots from the Spray glider occupation of the slope transect. Left to right the parameters are fChl in mg/m3, salinity in PSU, and temperature in °C with their associated color-bars directly right of the section. The vertical dimension is meters, seen on the far left. The white dots at 250 m depth are the latitudinal position of the deep chlorophyll profiles. The thin white (and black on the salinity plots) contour lines are isopycnals. The white circled region is a high chlorophyll, fresh and cool, water mass patch and the red line is the location of the Gulf Stream (GS) front with the GS to the south.

CHAPTER 5

DISCUSSION

5.1. METHODS AND ANALYSIS CRITIQUE

5.1.1. CALIBRATION DISCUSSION

Confidence in the southern MAB PEACH-fChl analysis was dependent upon cross calibration using the OC standard. The cross-calibration effectively scaled the fChl observations to a consistent standard measure of chlorophyll, the remotely sensed OC, which does not contain the calibration uncertainty across all the glider missions undertaken during the two year period. Evidence of this is in the reduction of cross-mission variability seen by the reduced standard deviation of the normalized mission means before to after the calibration. The uncertainty associated with OC's performance introduces some possibility that the OC standardization dampens natural fChl signals from chlorophyll at depth not captured by the OC remote sensing. However, the standardization is likely to only enhance accuracy of further analysis because OC retains many scales and variability of natural explainable seasonal chlorophyll phenomena in this region, like the seasonal modes observed by Xu et al. (2011). After observing reduction of variability by standardization to a common standard, OC, which contains natural phenomena and is not subjected to the systematic variability from multiple Spray glider missions employing multiple different SCFs, we can move forward with confidence that our analysis of using fChl is relatively precise.

The cross calibration improves our confidence in the PEACH-fChl with overall agreement with calibrated, independent *in situ* fChl data. This agreement was consistent when standard deviations of independent WOD and Sharp monthly binned profiles were lower relative

to other months and the number of profiles included were higher relative to other months; in order words, when the independent observations were their most robust. Furthermore, the proportion of mean monthly profiles with >4 profiles included in calculation, in depth zones where standard deviations were low relative to the rest of the profile, had highest agreement of all comparisons. This agreement in these specific scenarios is important support for the validation because a higher number of observations with lower standard deviation insinuates this area is a more robust representation of the system and less susceptible to discrepancies from outlying, ephemeral and episodic, dynamics. On the other hand, the discrepancies in vertical sections of profiles occurred where profiles exhibited the greatest standard deviation, in monthly profiles with a smaller sample size within the monthly bin. These profiles would be the least robust representation of the system and the most susceptible to ephemeral and episodic processes, relative to the other monthly profiles. Thus, they do not sufficiently invalidate agreement in the other profiles supporting validation of the calibration. From this consideration of relative variability in the independent fChl and PEACH-fChl, we can move forward with understanding that analysis conducted across missions is relatively accurate.

5.1.2. SPATIAL UNCERTAINTY OF THE PEACH SOUTHERN MAB CHLOROPHYLL DISTRIBUTIONS

Todd (2020a) used a weighted least squares regression and broad scale variability filtering to calculate the annual mean hydrographic distributions from the PEACH Spray glider program in the southern MAB. That method was used to account for forms of internal variability when using a moving platform, to weight the spatial output relative to spatiotemporal variability, and to generate a smoother picture with high-resolution gridded output.[27] The gridded product should be assumed to be closer to climatology, but still short thereof on basis that a complete

climatology requires a longer multiyear time series, than the spatial bin calculation method used in this study to achieve a comparable annual temporal bin mean distribution, with the addition of seasonal temporal bins and standard deviation calculations. Validating the choice to omit the weighting terms and broad scale filter, the annual mean salinity and temperature distributions calculated with our spatiotemporal bins (Supplementary Figure 1 and 2) have the same spatial features as the annual mean distributions presented in Todd (2020a). The agreement between the two methods of spatial averaging in hydrographic properties provides confidence moving forward using fChl distributions from the less sophisticated method of spatial analysis to make comparisons with other studies in the MAB.

The observing capacity of the PEACH Spray glider program was subject to spatial bias and uncertainty, limiting our confidence in the chlorophyll distributions. Repeat occupations were as much as 14 days apart, while in some cases, ephemeral chlorophyll enhancement in the MAB is known to occur on the timescales less than week (Oliver et al., 2022). All subsets seasonal and annual were observationally geospatially biased to central regions of the transects generally with nearly double the number of observations in center of each transect relative to either end (Supplementary Figure 3 through 6). Spatial bias due to different observational densities on the ends of the study domain were handled to some extent in the PEACH-fChl distribution by further refining the bounds of the distributions to 74.8 to 74.6°W and 35.75 to 36.75°N on shelf and slope, respectively. However, there is no way to handle the possibility that some chlorophyll variability is not resolved by the repeat PEACH occupations Additionally, seasonal subsets had geospatial bias that could affect their seasonal comparability and possible scaling of spatial mean and standard deviation features (Supplementary Figure 5 and 6). It is possible that these geospatial biases affect the results of this study, especially in shelf where

there is bias to the subsurface where a subsurface maximum was observed and on slope were geospatial differences where observed. However, the investigation into specific occupations provide confidence in the distributions, where many observed features in individual occupations are co-occurrent with mean and seasonal chlorophyll distribution features. Relative geospatial observation density maxima and minima in the seasonal distributions were co-occurrent with some annual and standard deviation PEACH-fChl geospatial features. This suggest potential that seasonal episodic dynamics could potentially affect how definitive features are in an ideal climatology of the both the annual and seasonal distributions, in contrast to what we observed here. That stated, the features resolved in distributions fit in the background context of the biogeochemical and hydrographic dynamics along the each transects path.

5.2. DYNAMICS FROM THE PEACH-FCHL TRANSECTS

The vertical structure of the annual mean and standard deviation of fChl had surface-to-subsurface maximums relative to respective depths of shelf and slope. At depths below these maximums, all the vertical structures exhibited decreased concentration of fChl as a function of depth. These vertical structures of fChl are typical of the Case 1 water euphotic dynamics, where light limitation primarily drives the distribution of chlorophyll (Morel et al., 1988). However, there were apparent (unquantified during this work) summer subsurface maximums and horizontal spatial differences in the rate or trend of decreasing chlorophyll concentration with depth along the slope that suggested other chlorophyll dynamics. These differences are likely associated the horizontal variability in physical characteristics across the study domain that drive different vertical structure of the optical field, distribution of nutrient abundance, and transport of chlorophyll to depth. To address this, we discuss how these differences are spatially coherent with known seasonal and hydrographic dynamics on the slope and shelf transects' path.

5.2.1. IMPLICATION OF PEACH-FCHL TRANSECTS SEASONALITY

The seasonally and depth resolved PEACH-fChl observations from the slope and shelf transect showed coherent features of seasonal contrast that aligned with regime shifts between seasons in previous the cruise based and integrated platform studies. The summer onset of stratification between two cruises in March and July 1997 observed by Lohrenz (2002) was expanded upon here.[16] There was a high MLD winter-spring season on both the slope and shelf with chlorophyll at greater depth and relatively high mean and standard deviation concentration fChl, ~1 mg m^{-3}, dispersed vertically across the water column. This transitioned to the low MLD summer season, with a more pronounced subsurface maximums with no increase in fChl concentration, relative to winter-spring, as coupled nutrient and light limitation likely isolates chlorophyll dynamics to the subsurface zone. This was followed by a significant reduction of chlorophyll in fall. Xu et al. (2011) also found that the magnitude of seasonal chlorophyll events in the MAB is influenced by water column stability, with connections to controls on light limitation in the euphotic zone. They observed two seasonal chlorophyll enhancement modes, fall-winter and spring, which are slightly out of phase with what we observed here. In their study using empirical orthogonal functions of OC, the first mode of chlorophyll associated with buoyant plumes and the frequency of storms in the fall-winter period and the second in spring with enhancement further offshore on slope.[30] When considering mean southward flow of the relative productive MAB toward Cape Hatteras throughout the year, a seasonal phase shift between two studies could connect fall, winter seasonal high chlorophyll further north with the slightly later winter-spring seasonal signal of high fChl and MLD in the southern MAB (Lentz, 2008). This potential link suggests the novel hypothesis that peak chlorophyll in southern MAB chlorophyll could be phase shifted with a lag relative to the rest of the MAB by 1-to-3 months,

coherent with phase shift of seasonal hydrographic dynamics transported in this region relative to the rest of the MAB. This is also supported by the first principal component mode observed in the mean circulation near Cape Hatteras is aligned with isobaths and oriented towards the Cape.[10] This further suggests that biogeochemical process and composition studies of MAB and SAB water, north and south of the Cape, are applicable to the origins of biogeochemical dynamics at the export hotspot (Todd, 2020a). This speculation suggests that the southern MAB and its adjacent systems north and southwest are biogeochemically connected through transport. However, it does not rule out possibility of regionally specific biogeochemical processes initiating independently with their regional seasonal dynamics. The next section dives into examples of specific chlorophyll distributions that are potentially associated with specific mechanisms of seasonal cross shelf transport observed in this region, which is the second principal component mode of mean water mass circulation near Cape Hatteras (Han et al., 2022).

5.2.2. INDICATIONS OF WINTER-SPRING EPISODIC CROSS SHELF EXCHANGE OF CHLOROPHYLL AT DEPTH ON SLOPE TRANSECT

On the slope transect, the convergence zone of episodic shelf water exchange directly north of the GS wall co-occurs with the initiation of the southward increase in fChl at depths of 150-to-250 m, as seen in the annual and winter-spring slope PEACH-fChl distributions, especially in the standard deviation distribution. Additionally, there is no chlorophyll reduction at and beyond the mean location of the GS wall, at ~35.75 °N, which is expected in oligotrophic GS waters relative to the southern MAB. Thereby suggesting a connection between seasonal physical ocean circulation drivers of variability across depths and the GS front to chlorophyll. Furthermore, given the unbroken distinct water mass features of the 10 studied events in section 4.2.3. It is likely that these drivers are happening on submeso-to-meso scales where mixing water

masses is still in the earlier stages; and with the connection to chlorophyll, the physical drivers of these patterns are tied to transport from the euphotic zone.

Export of chlorophyll rich shelf water has been observed in cold pool water as southward transport as part of the edge-frontal jet, which is then shunted eastward and entrained into the GS (Churchill and Gawarkiewicz, 2014). These observations were in the month of August when seasonal pycnocline and sub-pycnocline cold pool waters of the MAB are well developed. Cold pool water is remnant of winter water that was capped by the seasonal pycnocline formation. The few deep chlorophyll profiles during summer season when mixed layer depths were low could be due to the mechanism of cold pool water export. However, the median yearday distribution of deep chlorophyll observations from PEACH were in the winter-spring season, defined by larger mixed layer depths and high integrated chlorophyll, prior to the development of the seasonal pycnocline. This suggests a vertical chlorophyl transport mechanism to depths beyond the euphotic zone earlier in year, potentially on shorter timescales than the summer cold pool export.

One of the submeso-to-meso scale mechanisms that is driving chlorophyll from the shelf surface all the way to entrainment in the GS at greater depths, in days to weeks during the winter-spring season, are shelf water cascades (Han et al., 2021). The January 2019 event shown in Figure 14 is the event discussed by Han et al. (2021) and was detected by the deep chlorophyll event threshold used in this study. Using the features of the event described in Han as a template to compare other deep chlorophyll events, this analysis found that these events all share a cascade like features with the relatively cooler, fresher shelf water mass features adjacent to the GS. Deep chlorophyll, > 0.75 mg fChl m^{-3} at depths > 100 m, was distributed along the isopycnals and occurred in isolated regions of cool, fresh water at the frontal boundary much like the case observed by Han et al. (2021). The temperature-salinity diagram shown in Figure 11

supported this discovery with highest values of deep chlorophyll seen along the 26.5 g kg^{-1} isopycnals in the fresher, cooler end of the isopycnals in temperature-salinity space where the shelf and GS water may be exchanging at densities greater than GS densities at these depths (100-300 m, Figure 11). This integrative analysis shows that the shelf high chlorophyll water mass type, at depths between 100-to-300 m, that includes the labeled deep chlorophyll events are distributed along isopycnals where frontal episodic exchange, like shelf water cascades, are possible. Furthermore, these deep chlorophyll events are associated with the coldest and freshest water along those isopycnals, coherent with the background shelf water cascades in this region are temperature driven density reversals from surface cooling of fresh water adjacent to the GS (Han et al., 2021). Cascade mechanisms require preconditioning to density contrast, which can be assisted or hindered by salinity, temperature, and/or both temperature and salinity fronts due to horizontal advection.[27] It is likely, with the episodic character with cessation of exchange due to the shelf break and GS salinity fronts (Todd, 2020a) and the temperature cooling precursor to the regional shelf water cascade case study (Han et al., 2021), that this mechanism has the potential to be both hindered and assisted by multiple dynamics working simultaneously.

CHAPTER 6

CONCLUSIONS AND FUTURE WORK

Calibration of the PEACH-fChl transects in the southern MAB from Spray gliders using OC standard with exponential and dark offset provided novel opportunity to observe seasonally and depth resolved distributions of the mean and standard deviation of the multiyear transects, depicting both annual and seasonal dynamics, both along the slope and across the shelf. These distributions were grounded in the hydrographic and biogeochemical characteristics of this region, with vertical chlorophyll structures typical of the MAB and differences from the euphotic driven distributions of chlorophyll are associated with the development of the seasonal pycnocline and location of the GS frontal boundary.

This usage of the PEACH-fChl data could use refinement with more computational work by applying the weighted and broad scale filtering method described in Todd (2020a) to calculate the mean distributions on the standard deviation and mean of PEACH-fChl to better handle sources of spatial uncertainty from observational bias and internal variability using am moving platform.[27] That stated, this is also in line with the motivation of a sensitivity analysis, as the PEACH-fChl distributions considered here are averaged at scales greater than the filters applied by Todd (2020a) but may still be responsive to biased variability. Vectors from the 1-MHz Nortek AD2CP Doppler current profiler should be used to complement the fChl observations by computing chlorophyll flux, and flux should be considered in each of the deep events seen adjacent to the GS wall to suggest the potential of deep chlorophyll as a vector for export. Furthermore, these deep chlorophyll events may be constrainable to specific mechanisms with comprehensive dynamic analysis and numerical modeling techniques. Finally, this calibrated

PEACH-fChl could be instrumental in developing machine-learning methods to predict longer, more spatially, and depth resolved chlorophyll information in the southern MAB by integrating remote sensing sea surface temperature, sea surface height, and OC. Sammartino et al. (2020) reconstructed depth resolved chlorophyll, $R^2 = 0.71$, using those inputs in another geographical system using machine learn techniques. And in a preliminary build with the PEACH-fChl training set, we achieved an $R^2 = 0.63$ predicting depth integrated chlorophyll from OC predictors.

The larger features in the standard deviation than the mean, and the horizontal variability in the annual and seasonal vertical structure of fChl across the southern MAB, suggest that southern MAB chlorophyll is driven by seasonal, episodic ocean circulation drivers associated with the GS boundary. Winter-spring was the relative high of episodic chlorophyll, ~1 mg m^{-3} in the mean and standard deviation, season extending to the GS wall and contained "deep chlorophyll events" adjacent to the GS front. From examination of the water mass distributions, we hypothesize they're likely driven by submeso-to-mesoscale physical ocean circulation dynamics, like shelf water cascades and the shunting of the shelf break jet carrying MAB cold pool water. The seasonal dynamics high-resolution PEACH-fChl in the southern MAB suggest potential regime shifts between seasons: with a high chlorophyll content extending to greater depth on the slope and the shelf, reaching 237 m in one of the "deep chlorophyll events", in the winter-spring season; a stratified subsurface maximum in chlorophyll at 20 to 30 m across the entire southern MAB during summer season; and a low chlorophyll fall season. This study observed the likely episodic annual and seasonal depth distributions of chlorophyll in the southern MAB; providing novel insight into the potential magnitude of seasonal episodic export of chlorophyll to depth in the southern MAB and suggesting specific mechanism, shelf water

cascades, that could be a pathway for carbon sequestration through irreversible export and entrainment in the open ocean boundary current at significant depths below surface mixing processes.

REFERENCES

Bailey, S.W., & Werdell, P.J. (2006). A multi-sensor approach for the on-orbit validation of ocean color satellite data products. *Remote Sensing of Environment*, 102(1-2), 12-23. https://doi.org/10.1016/j.rse.2006.01.015

Bauer, J.E., Cai, W.-J., Raymond, P.A., Bianchi, T.S., Hopkinson, C.S., & Regnier, P.A.G. (2013). The Changing Carbon Cycle of the Coastal Ocean. *Nature,* 504(7478), 61-70. https://doi.org/10.1038/nature12857

Biscaye, P.E., Flagg, C.N., & Falkowski, P.G. (1994). The Shelf Edge Exchange Processes Experiment, SEEP-II: An Introduction to Hypotheses, Results and Conclusions. *Deep Sea Research Part II: Topical Studies in Oceanography,* 41(2), 231-52. https://doi.org/10.1016/0967-0645(94)90022-1

Boss, E., Swift, D., Taylor, L., Brickley, P., Zaneveld, R., Riser, S., Perry, M.J., & Strutton, P. G. (2008). Observations of Pigment and Particle Distributions in the Western North Atlantic from an Autonomous Float and Ocean Color Satellite. *Limnology and Oceanography,* 53(5.2), 2112-22. https://doi.org/10.4319/lo.2008.53.5_part_2.2112

Boyer, T.P., Baranova, O.K., Coleman, C., Garcia, H.E., Grodsky, A., Locarnini, R.A., Mishonov, A.V., Paver, C.R., Reagan, J.R., Seidov, D., Smolyar, I.V., Weathers, K., & Zweng, M.M. (2018). World Ocean Database 2018. A.V. Mishonov, Technical Ed., NOAA Atlas NESDIS 87. https://www.ncei.noaa.gov/sites/default/files/2020-04/wod_intro_0.pdf

Churchill, J.H., & Gawarkiewicz, G.G. (2014). Shelf Water and Chlorophyll Export from the Hatteras Slope and Outer Shelf. *Journal of Geophysical Research: Oceans*, 119(7), 4291-304. https://doi.org/10.1002/2014JC009809

De Boyer Montégut, C. (2004). Mixed Layer Depth over the Global Ocean: An Examination of Profile Data and a Profile-Based Climatology. *Journal of Geophysical Research*, 109(C12). https://doi.org/10.1029/2004JC002378

Fabry, V.J., Langdon, C., Balch, W.M., Dickson, A.G., Feely, R.A., Hales, B., Hutchins, D.A. et al. (2008). Present and future impacts of ocean acidification on marine ecosystems and biogeochemical cycles. In *Report of the Ocean Carbon and Biogeochemistry Scoping Workshop on Ocean Acidification Research*, La Jolla, California.

Friedrichs, M.A.M., St-Laurent, P., Xiao, Y., Hofmann, E., Hyde, K., Mannino, A., Najjar, R.G. et al. (2019). Ocean Circulation Causes Strong Variability in the Mid-Atlantic Bight Nitrogen Budget. *Journal of Geophysical Research: Oceans*, 124(1), 113-34. https://doi.org/10.1029/2018JC014424

Han L., Seim H., Bane, J., Savidge D., Andres M., Gawarkiewicz, G., & Muglia, M. (2022). Ocean Circulation Near Cape Hatteras: Observations of Mean and Variability. *Journal of Geophysical Research: Oceans,* 127(12). https://doi.org/10.1029/2022JC019274

Han L., Seim H., Bane, J., Todd, R.E., & Muglia, M. (2021). A Shelf Water Cascading Event near Cape Hatteras. *Journal of Physical Oceanography.* https://doi.org/10.1175/JPO-D-20-0156.1

Huthnance, J.M. (1995). Circulation, Exchange, and Water Masses at the Ocean Margin: The Role of Physical Processes at the Shelf Edge. *Progress in Oceanography,* 35(4), 353-431. https://doi.org/10.1016/0079-6611(95)80003-C

Ivanov, V.V., Shapiro, G.I., Huthnance, J.M., Aleynik, D.L., & Golovin, P.N. (2004). Cascades of Dense Water around the World Ocean. *Progress in Oceanography,* 60(1), 47-98. https://doi.org/10.1016/j.pocean.2003.12.002

Lavigne, H., D'Ortenzio, F., Claustre, H., & Poteau, A. (2012). Towards a Merged Satellite and *in Situ* Fluorescence Ocean Chlorophyll Product." *Biogeosciences*, 9(6), 2111-25. https://doi.org/10.5194/bg-9-2111-2012

Lentz, S.J. (2008). Observations and a Model of the Mean Circulation over the Middle Atlantic Bight Continental Shelf. *Journal of Physical Oceanography*, 38(6), 1203-21. https://doi.org/10.1175/2007JPO3768.1

Lohrenz, S.E., Redalje, D.G., Verity, P.G., Flagg, C.N., & Matulewski, K.V. (2002). Primary Production on the Continental Shelf off Cape Hatteras, North Carolina. *Deep Sea Research Part II: Topical Studies in Oceanography*, 49(20), 4479-509. https://doi.org/10.1016/S0967-0645(02)00126-1

Morel, A., & Loisel, H. (1998). Apparent Optical Properties of Oceanic Water: Dependence on the Molecular Scattering Contribution. *Applied Optics*, 37(21), 4765. https://doi.org/10.1364/AO.37.004765

Najjar, R.G., Herrmann, M., Alexander, R., Boyer, E.W., Burdige, D.J., Butman, D., Cai, W.-J. et al. (2018). Carbon Budget of Tidal Wetlands, Estuaries, and Shelf Waters of Eastern North America. *Global Biogeochemical Cycles*, 32(3), 389-416. https://doi.org/10.1002/2017GB005790

NASA Ocean Biology Processing Group. (2017). VIIRS-SNPP Level 2 Ocean Color Data. Version R2018.0. NASA Ocean Biology DAAC. https://doi:10.5067/NPP/VIIRS/l2/OC/2018.

Oliver, H., Zhang, W.G., Archibald, K.M., Hirzel, A.J., Smith, W.O., Sosik, H.M., Stanley, R.H.R., & McGillicuddy, D.J. (2022). Ephemeral Surface Chlorophyll Enhancement at the New England Shelf Break Driven by Ekman Restratification. *Journal of Geophysical Research: Oceans*, 127(1). https://doi.org/10.1029/2021JC017715

Palevsky, H., Clayton, S., Atamanchuk, D., Battisti, R., Batryn, J., Bourbonnais, A., Briggs, E.M. et al. (2022). *OOI Biogeochemical Sensor Data Best Practices and User Guide.* Version 1.0.0. https://doi.org/10.25607/OBP-1865

Sammartino, M., Nardelli, B.B., Marullo, S., & Santoleri, R. (2020). An Artificial Neural Network to Infer the Mediterranean 3D Chlorophyll-a and Temperature Fields from Remote Sensing Observations. *Remote Sensing*, 12(24), 4123. https://doi.org/10.3390/rs12244123

Seapoint Chlorophyll Fluorometer: Ocean Profiling, Water Quality, Biomass, Nutrients, and more. (n.d.). On Seapoint Sensors' online website. Retrieved from http://www.seapoint.com/scf.htm

Seim, H.E., Savidge, D., Andres, M., Bane, J., Edwards, C., Gawarkiewicz, G., He R. et al. (2022). OVERVIEW OF THE PROCESSES DRIVING EXCHANGE AT CAPE HATTERAS PROGRAM. *Oceanography,* 35(2).

Selden, C.R., Chappell, P.D., Clayton, S., Macías-Tapia, A. Bernhardt, P.W., & Mulholland, M.R. (2021). A Coastal N_2 Fixation Hotspot at the Cape Hatteras Front: Elucidating Spatial Heterogeneity in Diazotroph Activity via Supervised Machine Learning. *Limnology and Oceanography*, 66(5), 1832-49. https://doi.org/10.1002/lno.11727

Shapiro, G. I., & Hill A.E. (1997). Dynamics of Dense Water Cascades at the Shelf Edge. *Journal of Physical Oceanography,* 27(11), 2381-94. https://doi.org/10.1175/1520-0485(1997)027<2381:DODWCA>2.0.CO;2

Todd, R.E. (2020a). Export of Middle Atlantic Bight Shelf Waters Near Cape Hatteras From Two Years of Underwater Glider Observations. *Journal of Geophysical Research:* Oceans, 125(4). https://doi.org/10.1029/2019JC016006

Todd, Robert E. (2020b). Spray Glider Observations in Support of PEACH. Scripps Institution of Oceanography, Instrument Development Group. https://doi.org/10.21238/S8SPRAY0880

Wood, A.M., Sherry, N.D., & Huyer, A. (1996). Mixing of Chlorophyll from the Middle Atlantic Bight Cold Pool into the Gulf Stream at Cape Hatteras in July 1993. *Journal of Geophysical Research: Oceans,* 101(C9), 20579-93. https://doi.org/10.1029/96JC01135

Xu, Y., Chant, R., Gong, D., Castelao, R., Glenn, S., & Schofield, O. (2011). Seasonal Variability of Chlorophyll a in the Mid-Atlantic Bight. *Continental Shelf Research,* 31(16), 1640-50. https://doi.org/10.1016/j.csr.2011.05.019

Zaneveld, J.R.V., Barnard, A.H., & Boss, E. (2005). Theoretical Derivation of the Depth Average of Remotely Sensed Optical Parameters. *Optics Express,* 13(22), 9052. https://doi.org/10.1364/OPEX.13.009052

APPENDIX

Supplementary Table 1. Mission Calibration Parameters.

Mission Number	Multiplicative Gain Correction Factor	Gain Regression Root Mean Square	Power	Exponential Offset	Exponential Amplitude	Exponential Time Scale (Days)
1	0.36	0.19	1	0.071	0.027	20.655
2	0.93	0.24	1	0.104	0.138	8.672
3	0.66	0.38	1	0.057		
4	0.88	0.19	1	0.068		
5	0.90	0.09	1	0.246	-0.159	0.336
6	0.78	0.22	1	0.209		
7	0.50	0.17	1	0.061	0.025	3.99
8	5.89	0.45	1	0.076	0.065	49.659
9	1.96	0.24	1	0.06	0.013	2.548
10	0.70	0.08	1	0.095		
11	2.13	0.08	1	0.07		
12	5.48	0.37	1	0.096	0.055	61.691
13	0.28	0.18	1	0.106	0.064	3.146
14	0.57	0.30	1	0.172		
15	5.34	0.16	1	0.083	0.016	31.738

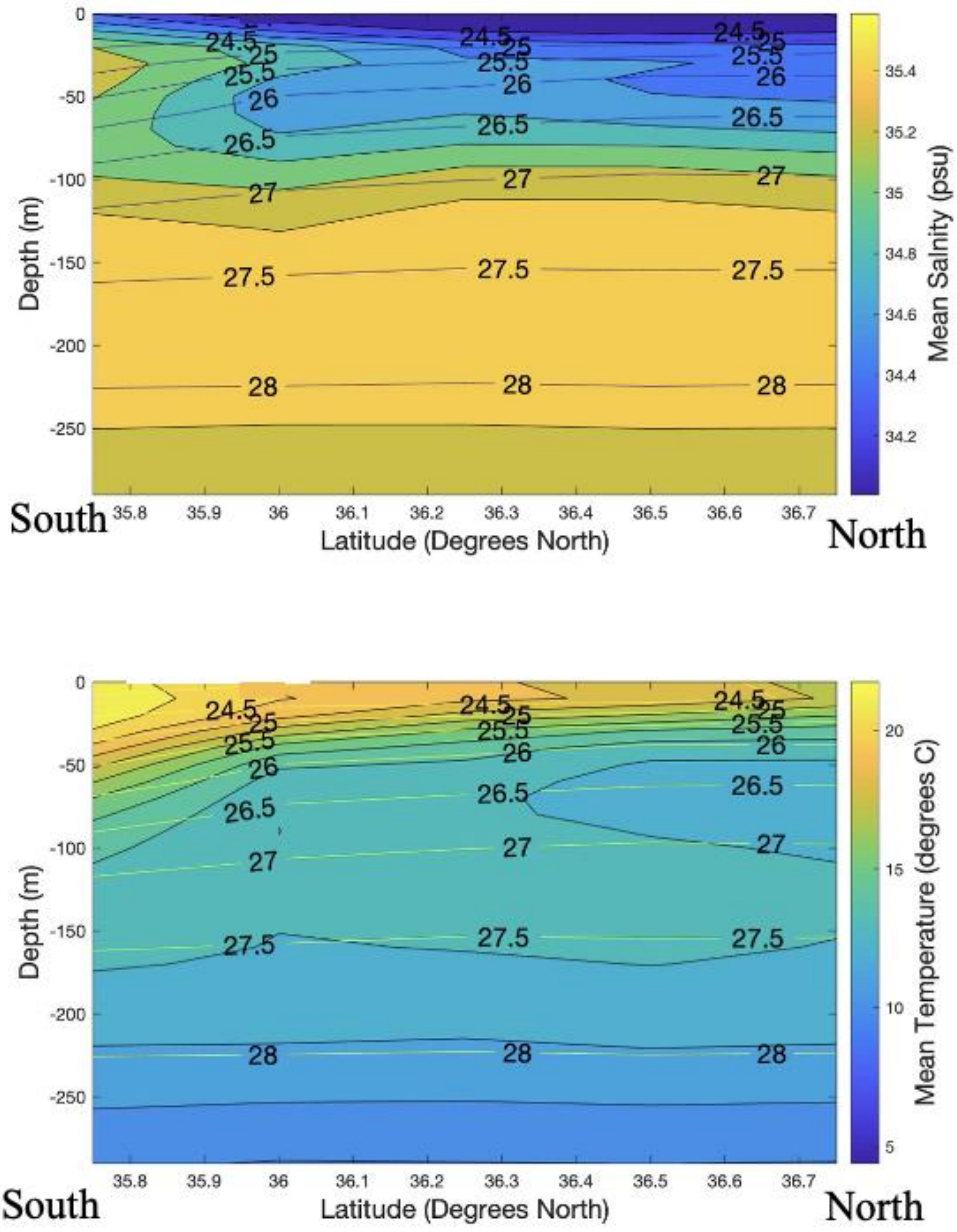

Supplementary Figure 1. Slope Salinity and Temperature Annual Mean. Spatially binned annual mean of salinity and temperature (top and bottom) from the slope occupations as a function of depth and latitude. These are in 10 m depth by 0.35°N bins. The white contours are isopycnals of mean and standard deviation, left and right respectively, potential density in units of kg m^{-3}.

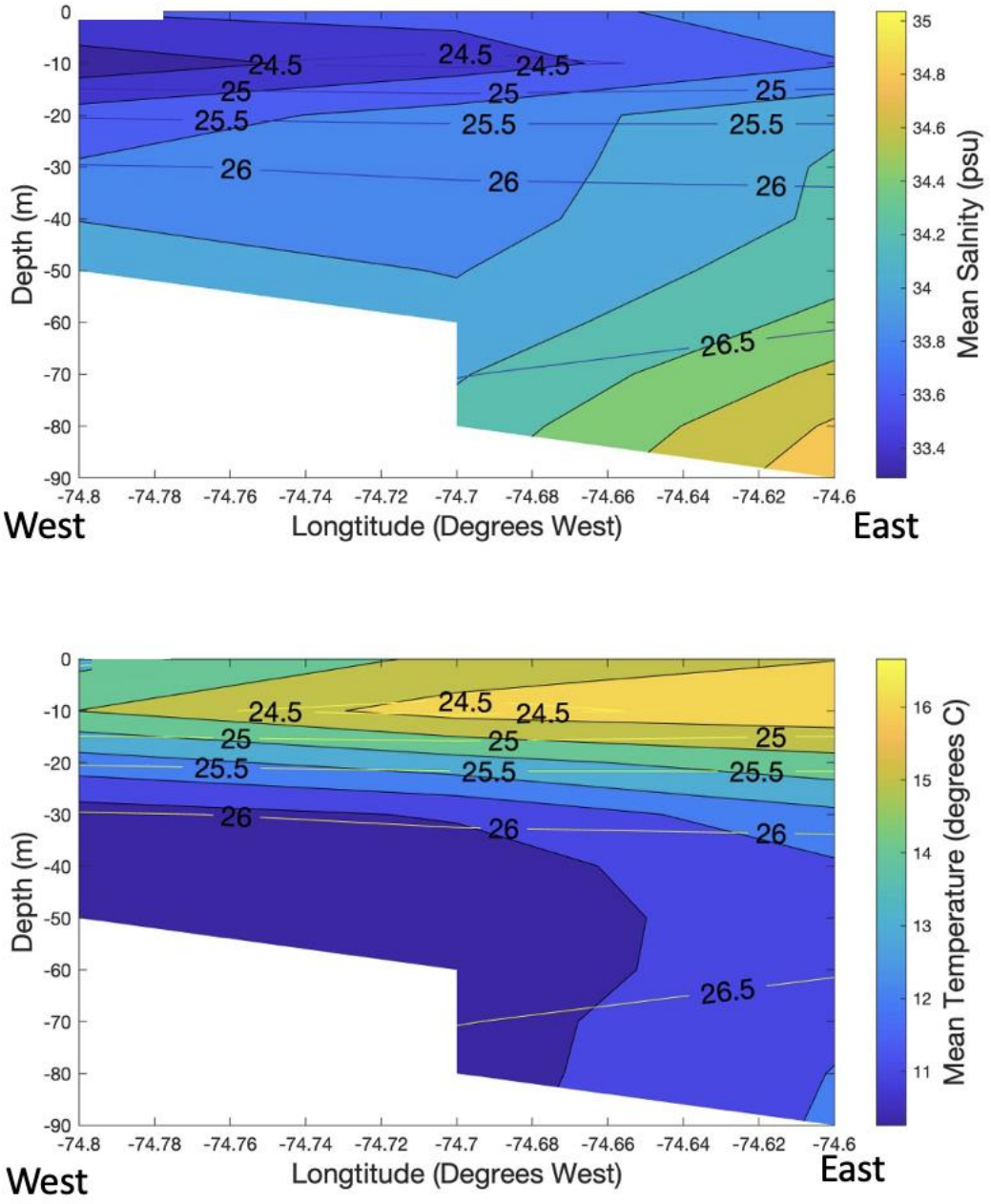

Supplementary Figure 2. Shelf Salinity and Temperature Annual Mean. Spatially binned annual mean of salinity and temperature (top and bottom) from the shelf occupations as a function of depth and longitude. These are in 10 m depth by 0.1°W bins. The white contours are isopycnals of mean potential density in units of kg m^{-3}.

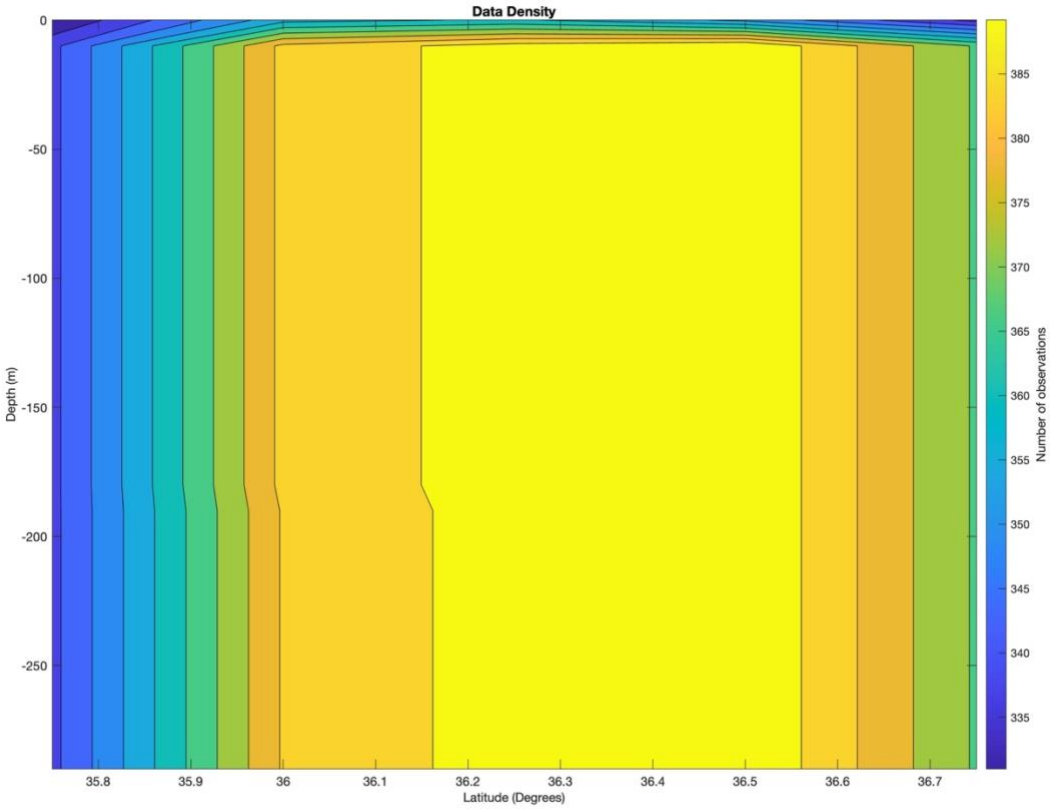

Supplementary Figure 3. Spatially binned annual data density of the slope occupations as a function of depth and latitude. These are in 10 m depth by 0.25°N bins.

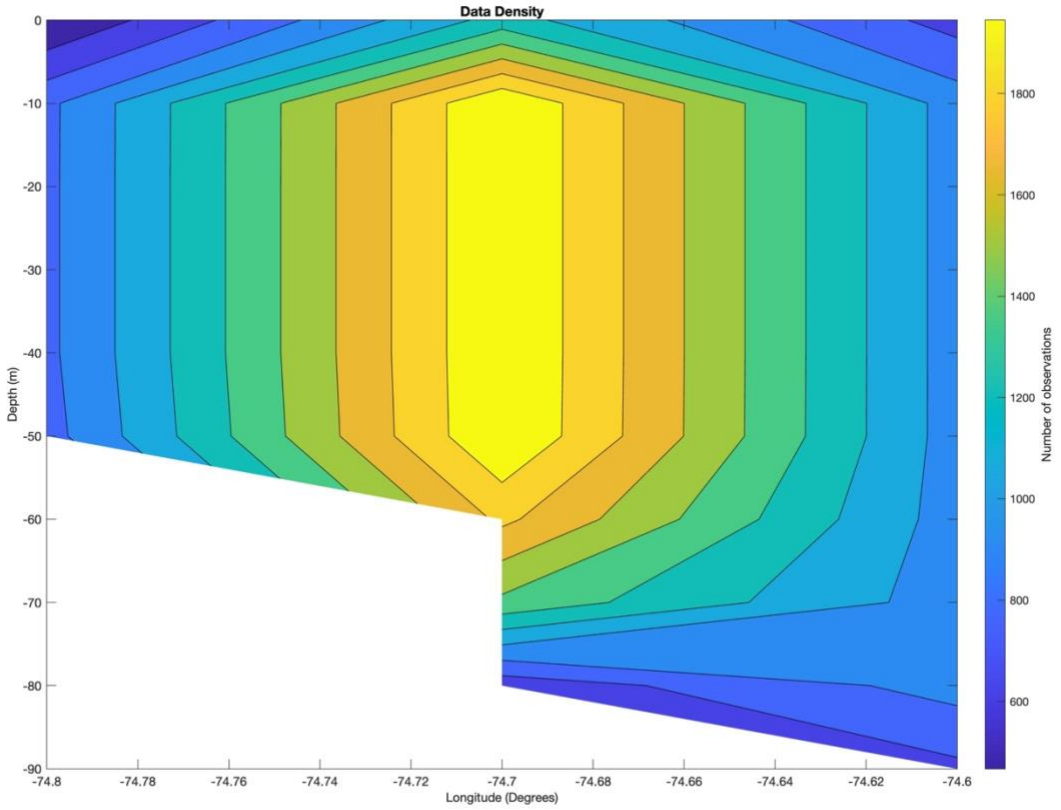

Supplementary Figure 4. Spatially binned annual data density of the shelf occupations as a function of depth and longitude. These are in 10 m depth by 0.1°W bins.

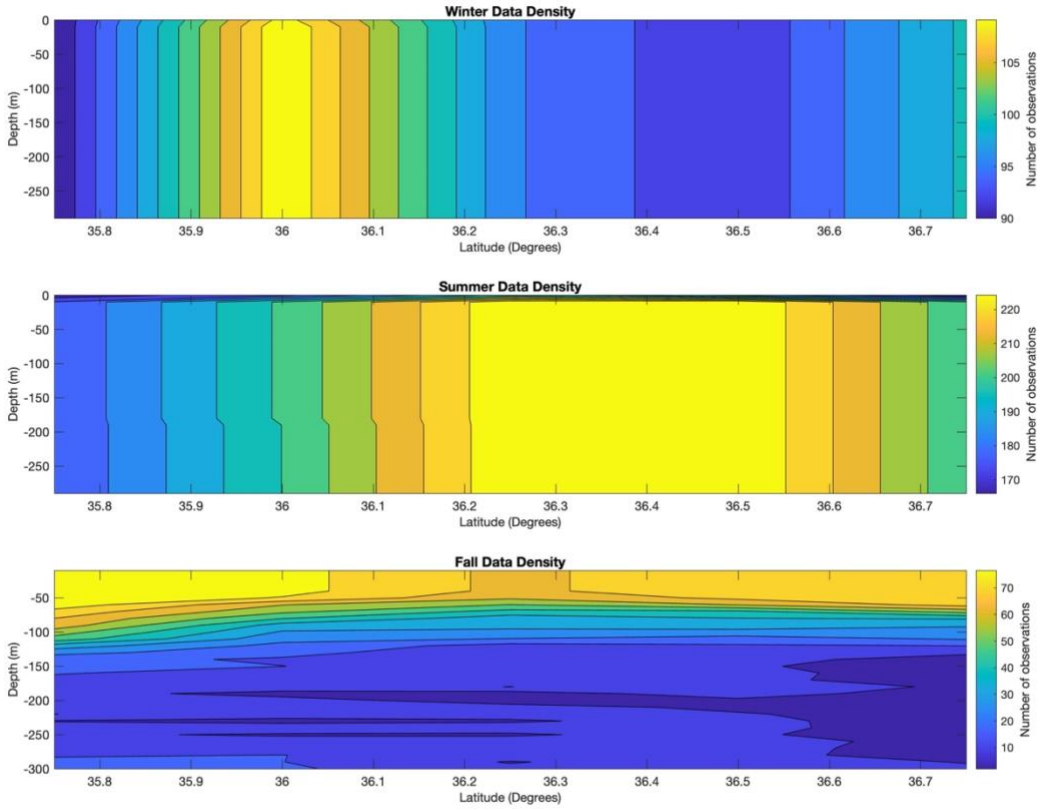

Supplementary Figure 5. Spatially binned seasonal data density of the slope occupations as a function of depth and latitude. These are in 10 m depth by 0.25°N bins. Seasons are distinguished based on the seasonal groups used in this study.

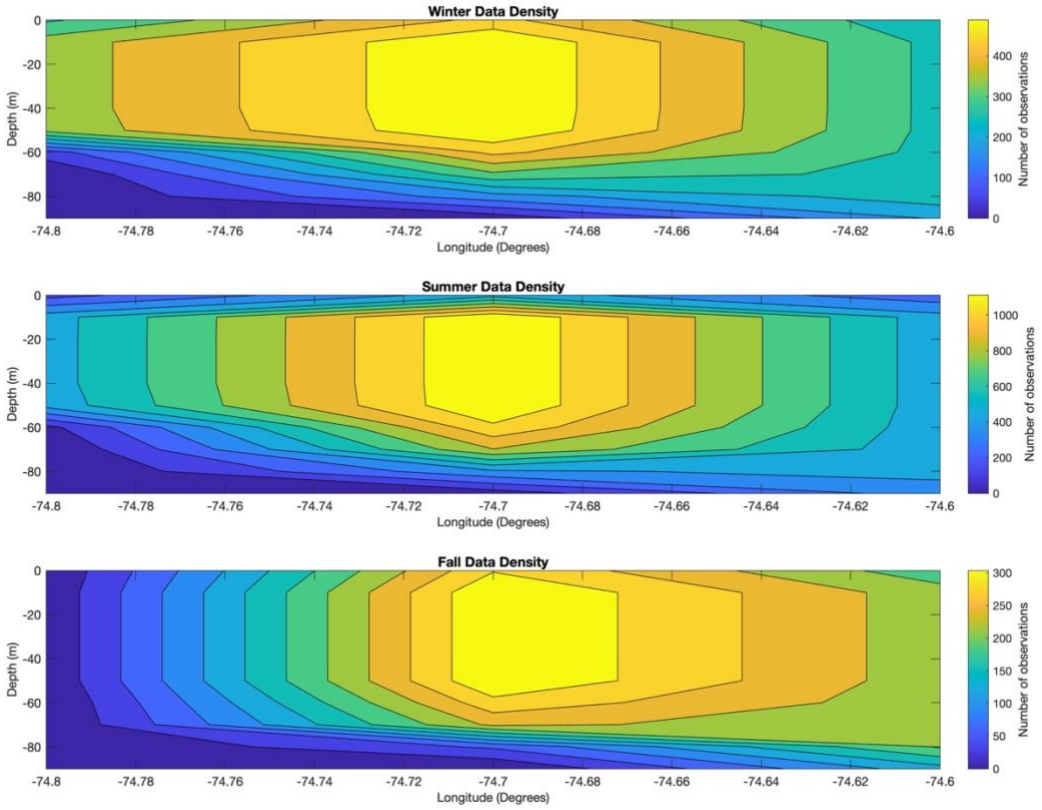

Supplementary Figure 6. Spatially binned seasonal data density of the shelf occupations as a function of depth and latitude. These are in 10 m depth by 0.25°N bins. Seasons are distinguished based on the seasonal groups used in this study.

VITA

Francesco Lane
University Email: flane002@odu.edu
Personal Email: francescojlane@gmail.com
Primary Phone: (352) 214-9770

Education

Master of Science – Ocean and Earth Sciences (Anticipated graduation: December 2023)
Old Dominion University's Ocean and Earth Sciences Department (ODU-OES)
Oceanography and Physics Bldg, 4394-4402 Elkhorn Ave, Norfolk, VA 23508, USA
Research Advisor: Dr. Margaret R. Mulholland (ODU-OES)

Bachelor of Science – Chemistry Major (Graduated: May 2018)
University of Florida – Innovation Academy
330 Newell Dr, Gainesville, FL 32603, USA

Work & Research Experience

Graduate Teaching Assistant at ODU-OES, Spring 2022 to Spring 2023.
Research Assistant at ODU-OES, Fall 2020 to Fall 2023
Operations Assistant at Carbonxt, Inc., Spring 2019 to Spring 2020
Undergraduate Researcher at Whitney Marine Biosciences Laboratory, August 2015 to December 2015

Publications and Presentations

Lane, F, S Clayton, RE Todd. Climatology of Chlorophyll in the Southern Mid-Atlantic Bight from PEACH Spray Gliders. In Preparation

Lane, F, S Clayton, RE Todd. Deep Chlorophyll as a Tracer of Winter Carbon Export at the Hatteras Front. OCB Summer Workshop. June 20-23, 2022. Woods Hole Oceanographic Institute. https://doi.org/10.5281/zenodo.6780544

Lane, F, S Clayton, RE Todd. Estimating biogeochemical exchanges at the Southern Mid-Atlantic Bight shelf break from glider transects. Ocean Sciences Meeting. February 27 - March 4, 2022. Virtual.

Lane, F, T Schafer, TZ Osborne. Black Mangroves and Smooth Cordgrass comparative study on the primary nutrient productivity, decomposition, and consumption in respect to the northern migration of mangroves in Florida Salt Marsh. Science by the Shore Student and Post-doctoral Symposium at Whiney Marine Bioscience Laboratory. May 20th, 2017. Marineland, FL.